AD-A153 748 UTILIZATION OF THE SEASAT SCATTEROMETER WINDS FOR OCEAN MIXED LAYER MODELING(U) NAVAL POSTGRADUATE SCHOOL MONTEREY CA E J COOLBAUGH DEC 84 1/2

UNCLASSIFIED F/G 8/3 NL

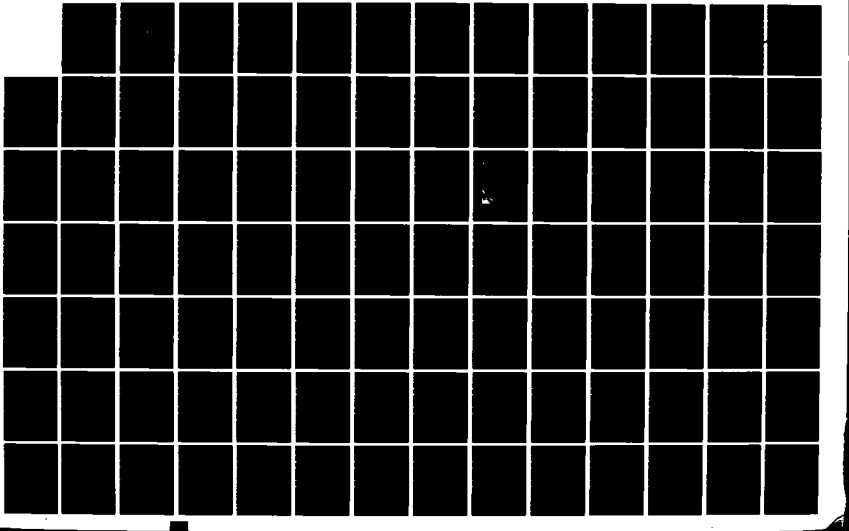

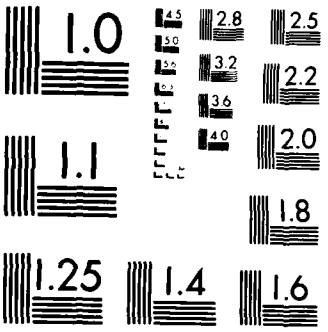

NAVAL POSTGRADUATE SCHOOL

Monterey, California

THESIS

UTILIZATION OF THE SEASAT SCATTEROMETER WINDS FOR OCEAN MIXED LAYER MODELING

by

Eric J. Coolbaugh

December 1984

Thesis Advisor: R.W. Garwood, Jr.

Approved for public release; distribution unlimited.

SECURITY CLASSIFICATION OF THIS PAGE (When Data Entered)

REPORT DOCUMENTATION PAGE		READ INSTRUCTIONS BEFORE COMPLETING FORM
1. REPORT NUMBER	2. GOVT ACCESSION NO. AD-A153 748	3. RECIPIENT'S CATALOG NUMBER
4. TITLE (and Subtitle) Utilization of the SEASAT Scatterometer Winds for Ocean Mixed Layer Modeling		5. TYPE OF REPORT & PERIOD COVERED Master's Thesis; December 1984
		6. PERFORMING ORG. REPORT NUMBER
7. AUTHOR(s) Eric J. Coolbaugh		8. CONTRACT OR GRANT NUMBER(s)
9. PERFORMING ORGANIZATION NAME AND ADDRESS Naval Postgraduate School Monterey, California 93943		10. PROGRAM ELEMENT, PROJECT, TASK AREA & WORK UNIT NUMBERS
11. CONTROLLING OFFICE NAME AND ADDRESS Naval Postgraduate School Monterey, California 93943		12. REPORT DATE December 1984
		13. NUMBER OF PAGES 100
14. MONITORING AGENCY NAME & ADDRESS(if different from Controlling Office)		15. SECURITY CLASS. (of this report) Unclassified
		15a. DECLASSIFICATION/DOWNGRADING SCHEDULE

16. DISTRIBUTION STATEMENT (of this Report)

Approved for public release; distribution unlimited.

17. DISTRIBUTION STATEMENT (of the abstract entered in Block 20, if different from Report)

18. SUPPLEMENTARY NOTES

19. KEY WORDS (Continue on reverse side if necessary and identify by block number)

Ocean Mixed Layer Modeling
SEASAT Scatterometer
FNOC and SASS Wind Comparison
SASS Wind Utilization

20. ABSTRACT (Continue on reverse side if necessary and identify by block number)

A study of the feasibility of using SEASAT Scatterometer wind measurements as the surface wind stress forcing for an ocean mixed layer model. Comparisons are made of daily SASS and FNOC winds and the respective mixed layer model results on a 2 degree latitude by 5 degree longitude grid from July 15 to August 15, 1978 in the Anomaly Dynamics Study region of the North Pacific Ocean. The direct comparison of the SASS and

DD FORM 1 JAN 73 1473 EDITION OF 1 NOV 65 IS OBSOLETE

S N 0102-LF-014-6601

SECURITY CLASSIFICATION OF THIS PAGE (When Data Entered)

Block #20 cont.

FNOC wind fields showed good agreement. Cases of reduced pattern correlation between the SASS and FNOC winds appear to result from periods of low percentage coverage by the SASS wind fields and the difference in spatial resolution between the SASS and FNOC winds. The results of the model comparison of the wind fields show the model's high sensitivity to the accuracy of its wind speed boundary condition. Nevertheless, the SASS and FNOC winds gave similar model results, demonstrating the potential of scatterometer wind speed measurements for use with future ocean mixed layer model prediction.

Approved for public release; distribution unlimited

Utilization of the SEASAT Scatterometer Winds for Ocean Mixed Layer Modeling

by

Eric J. Coolbaugh
Lieutenant, United States Navy
B.S., Florida Institute of Technology, 1978

Submitted in partial fulfillment of the
requirements for the degree of

MASTER OF SCIENCE IN METEOROLOGY AND OCEANOGRAPHY

from the

NAVAL POSTGRADUATE SCHOOL
December, 1984

Author: _____
Eric J. Coolbaugh

Approved by: _____
R.W. Garwood, Thesis Advisor

_____
P. Gallacher, Second Reader

_____
C.N.K. Mooers, Chairman,
Department of Oceanography

_____
John N. Dyer,
Dean of Science and Engineering

ABSTRACT

A study is made of the feasibility of using SEASAT Scatterometer wind measurements as the surface wind stress forcing for an ocean mixed layer model. Comparisons are made of daily SASS and FNOC winds and the respective mixed layer model results on a 2 degree latitude by 5 degree longitude grid from July 15 to August 15, 1978 in the Anomaly Dynamics Study region of the North Pacific Ocean. The direct comparison of the SASS and FNOC wind fields showed good agreement. Cases of reduced pattern correlation between the SASS and FNOC winds appear to result from periods of low percentage coverage by the SASS wind fields and the difference in spatial resolution between the SASS and FNOC winds. The results of the model comparison of the wind fields show the model's high sensitivity to the accuracy of its wind speed boundary condition. Nevertheless, the SASS and FNOC winds gave similar model results, demonstrating the potential of scatterometer wind speed measurements for use with future ocean mixed layer model prediction.

TABLE OF CONTENTS

LIST OF TABLES

LIST OF FIGURES

ACKNOWLEDGEMENTS

The author thanks the Jet Propulsion Laboratory for providing the SASS wind vector data set. The data archiving division of the Fleet Numerical Oceanography Center (FNOC) provided the FNOC wind data and surface pressure charts used in this study. Thanks go to Dr. Warren White and Dr. Steve Pazan, NORPAX data manager, for providing the TRANSPAC analyses of ocean thermal structure. A very special thanks to Mr. Patrick C. Gallacher for spending his valuable time and energy assisting the author in defining the goals, structure and scope of this study, as well as for his critical review of the manuscript. Appreciation is extended to Mr. Mike McDermet for providing archived GOES imagery. The computing was done at the W.R. Church Computer Center.

The author would like to express gratitude and thanks to Dr. Roland W. Garwood, Jr. for providing the ocean mixed layer model, as well as his expert guidance and encouragement during the preparation of this thesis.

Finally, and most certainly, I give my deepest love and gratitude to my wife, Kim, for devoting the word processing skill, time, energy, and love which made the completion of this thesis possible.

TABLE 1
Distribution of SASS Wind Speed Records with Incidence Angle

Angle	Wind Speed (m/s)										
	0-5	5-10	10-15	15-20	20-25	25-30	30-35	35-40	40-45	45-50	=50
0-5	3628	11255	6264	1195	276	116	77	39	28	21	52
5-10	67	264	132	29	7	3	0	2	0	0	1
10-15	0	0	0	0	0	0	0	0	0	0	0
15-20	0	0	0	0	0	0	0	0	0	0	0
20-25	1050	2491	1122	115	4	0	1	1	0	0	0
25-30	7954	16409	6031	409	0.	3	0	1	0	1	0
30-35	11621	19752	6863	573	13	0	1	0	1	1	1
35-40	9747	15350	5741	466	20	0	0	1	0	0	0
40-45	2144	20476	9113	860	59	1	0	1	0	0	0
45-50	1044	23665	11372	944	80	1	0	0	0	0	0
50-55	8338	23885	13233	889	71	6	1	1	0	1	0
55-60	337	1526	1121	84	4	2	0	0	0	0	0
60-65	0	0	0	0	0	0	0	0	0	0	0

improved screen for records which are most probably in error:

(1) Measurements made with incidence angles of less than 20 degrees were rejected.

(2) Measurements made with incidence angles exceeding 50 degrees were rejected.

(3) Measurements derived from signals with mixed polarization were rejected.

(4) Wind speed measurements exceeding 25 m/s were rejected.

The box in Table 1 encloses the records remaining after imposing criteria (1) and (2). Imposing criterion (3) alone eliminates 37,767 records, 92% of which were filtered out by the first two criteria. Criterion (3) does not eliminate any wind speed measurements greater than 25 m/s which were not eliminated by the first two criteria.

All wind speed measurements were calculated using a single functional form developed by Wentz (1977), which relates wind speed to backscattered irradiance. This algorithim was not verified by ground truth for wind speeds exceeding 25 m/s (Boggs, 1982). There were 15 wind speed measurements in excess of 25 m/s which were not eliminated by criteria (1), (2) or (3). Table 2 summarizes the characteristics of these 15 measurements and any possible association they may have with synoptic events visible from GOES imagery. Only three of the fifteen records contained known AACC, while the majority of the remaining records were

(4) Separate empirical algorithims for calculating wind speeds are used depending on the polarization of the signal from the fore and aft antenna. Thus, wind speed measurements derived from one horizontally and one vertically polarized signal are more likely to be in error (Peter Woiceshyn, personnal communication). Of the 268,458 records, 37,767 records (14% of the data) were derived with mixed polarization.

(5) The attenuation coefficient allows the reflected microwave signal to be corrected for attenuation due to atmospheric moisture. When the attenuation is unknown, wind speed measurements are subject to error from atmospheric moisture (Moore, et al., 1982). The total amount of atmospheric moisture was sensed by the SMMR (also aboard SEASAT) simultaneously with surface winds sensed by SASS. The moisture sensing was largely restricted to the right swath of the SASS path.

The attenuation coefficient for 136,007 (51%) of the data records was unknown for either the fore or aft antenna. For 6,204 records, the forward Antenna Attenuation Correction Coefficient (AACC) was known, and the aft AACC was unknown (only 18 of these required a correction to be made to the sensed radiation strength). There were no measurements with the aft AACC known and the forward AACC unknown. The AACC for both antennas was known for 102,236 records and required no correction to the return microwave signal. The remaining 555 records were corrected for attenuation, which was known for both the fore and aft antennas. Exclusion of all data with an unknown AACC is impractical. However, correcting the wind speed for those records with known AACC could improve the results.

Knowledge of these data set properties resulted in the following quality control criteria being imposed as an

absolute values derived for these regions are the most uncertain.

Several quality control restrictions were therefore imposed by JPL on the SASS data set. Two of these were used initially in this study:

(1) only wind speeds solutions of 50 m/s or lower were accepted as possible aliased solutions;

(2) only wind speed solutions derived from measurements with incidence angles of 70 degrees or less were accepted.

Examination of the entire data set revealed 54 wind speed solutions with a value of 50 m/s. These high wind speeds are unlikely for the mid-latitude North Pacific in August and suggested the need to impose additional quality control measures. The following potential errors in SASS measurements were identified:

(1) Wind speeds measured at low incidence angles, 20 degrees or less (i.e., the nadir swath), have a high probability of error (Boggs, 1982). The reliability of the Bragg scattering relationship decreases rapidly as the incidence angle of the radiation decreases below 20 degrees (i.e., as it becomes more perpendicular to the sea surface).

(2) Wind speeds measured at high incidence angles tend to have erroneously large values. Although initial screening allowed incidence angles as high as 70 degrees, angles above 50 degrees frequently yield erroneous wind speed values (Halberstam, 1980 and Boggs, 1982).

(3) The accuracy of wind speeds exceeding 25 m/s is questionable because of a lack of ground truth data to construct an empirical algorithm for those speeds (Boggs, 1982).

2. Quality Control Restrictions

Many studies have examined the quality of the SASS data. Jones et al. (1982) and Brown et al. (1982) verified that SASS wind speeds met the specifications of plus or minus 2 m/s or 10% of the wind speed. Hawkins and Black (1983) made a verification for near gale force winds of 17-18 m/s with similar results. Halberstam (1980) found that deriving wind speeds at a standard height reduced the effects of stability for an unstable atmosphere. However, Brown (1983) pointed to the need for an empirical algorithm for unstable atmospheric layers which better defined mesoscale disturbances, such as fronts. Such an algorithm would allow measurements to be adapted to regional mesoscale variations; otherwise, errors would be produced. Boggs (1982) has suggested further constraints on SASS data use, including cautious use of wind speed measurements exceeding 25 m/s.

With few exceptions, these studies indicate that the SASS wind speed measurements are as accurate as conventional in situ wind speed measurements when and where they have been compared. However, caution is necessary in accepting all measured values due to the uncertainty of derived results dependent on unknown atmospheric stablity. The SASS is able to resolve mesoscale disturbances which have regions of sharply defined gradients, although the

believed sufficient to resolve synoptic variability in wind stress).

E. THE SASS SURFACE WIND BOUNDARY CONDITION

1. Background

The SEASAT satellite carried four remote-sensing instruments, in addition to the scatterometer. SEASAT was launched into a nearly circular polar orbit with an approximate altitude of 800 km. SASS was enabled from 1800Z July 6 to 0200Z October 10, 1978, and was designed to cover 95 percent of the globe every 36 hours.

The SASS wind measurements were obtained for this study from the Jet Propulsion Laboratory (JPL) Pilot Ocean Data System (PODS). The data records were chosen to coincide with the ADS grid (Fig. 2). Since only wind speed is necessary to derive the wind stress at the sea surface, the the wind direction provided by SASS was neglected. Thus, the problem of aliased wind directions, which possibly complicates usage of the SASS wind measurements, is avoided. The wind speed values associated with aliased wind vector measurements "usually fall within a few percent of each other" (Boggs, 1982), so they were averaged to give one wind speed value for each data record. The SASS wind speed values have a reference height of 19.5m, as do the FNOC winds, and are calculated assuming an atmospheric boundary layer with neutral stability.

the monthly spatial and temporal scales of the initialization field are 5 degrees of longitude by 2 degrees of latitude.

C. THE SURFACE HEAT FLUX BOUNDARY CONDITION

The FNOC fields used to define heat flux boundary conditions in earlier studies of the ocean mixed layer have proven to be inadequate and have been replaced by climatological heat flux fields (Jaramillo, 1984) based on a monthly climatology of the North Pacific (Wyrtki, 1965).

D. THE FNOC SURFACE WIND BOUNDARY CONDITION

The FNOC wind forcing fields have been derived from archived FNOC six hourly analysis and prediction fields. These fields have been interpolated using a two dimensional fifth degree polynomial to hourly time intervals and projected onto an 11 by 41 grid (Gallacher, 1979). This grid coincides with the ADS region defined in Fig. 2.

The spatial scale of the FNOC winds is that of the 63 by 63 polar stereographic grid (true at 60N) used by the FNOC Northern Hemisphere atmospheric model. This spatial scale, though it varies with latitude, is adequate to resolve the atmospheric synoptic scale and is of the order of 300km at 40N. The temporal scale is 6 hours because these fields were archived with this periodicity. (This is

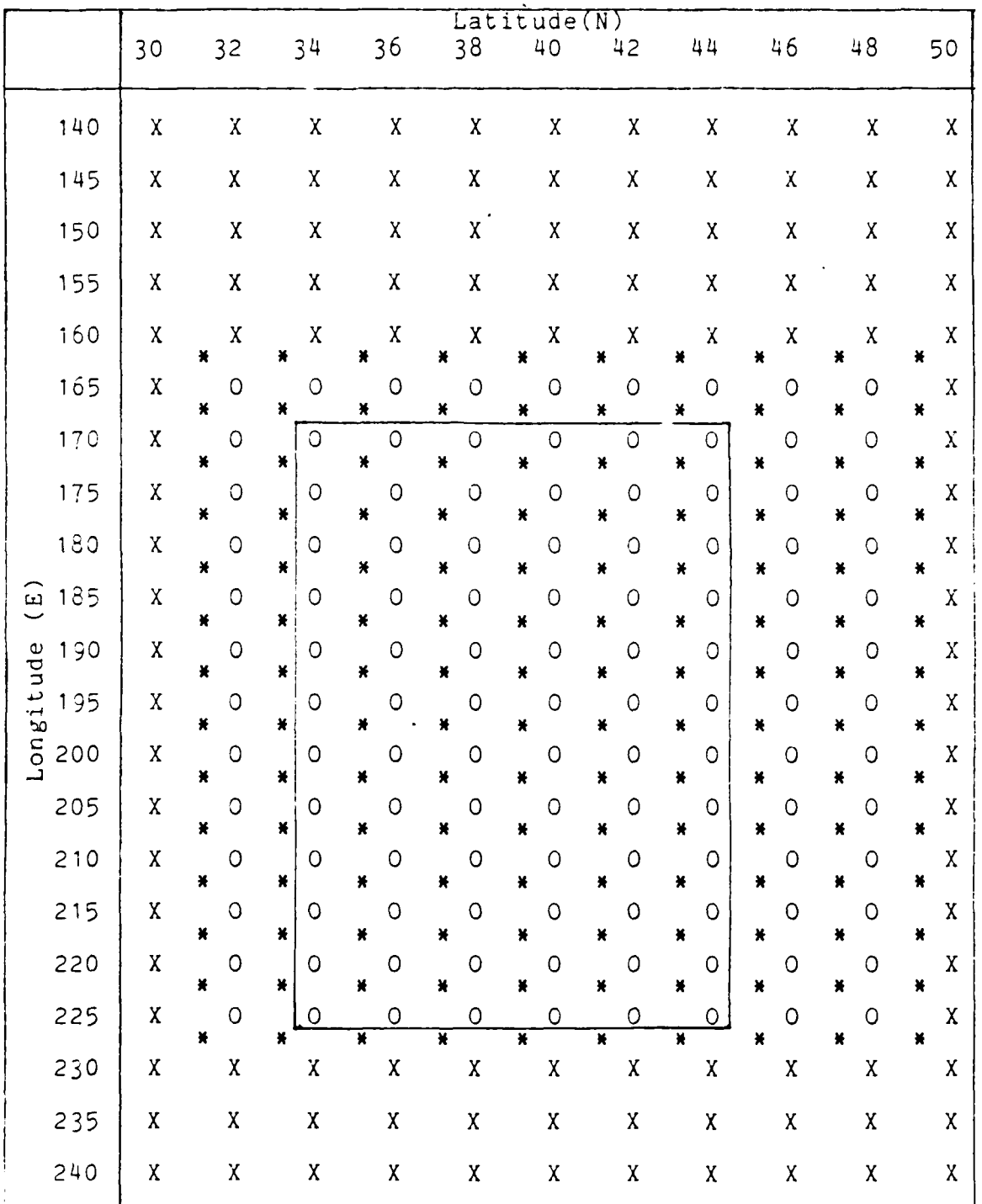

Figure 2. The ADS grid points ("X" and "O"), SASS data bin centers before interpolation ("*") and the reduced ADS grid (enclosed by a box).

II. DESCRIPTION OF INITIAL AND BOUNDARY CONDITIONS

A. BACKGROUND

The model requires a three-dimensional field of ocean temperature for initialization and verification. The surface heat flux and surface wind stress must be specified or known functions of time. The ocean thermal structure and the surface heat flux will be discussed briefly, then the FNOC and SASS wind fields will be discussed and contrasted.

B. THE MODEL INITIALIZATION AND VERIFICATION FIELDS

The model requires a data field which describes the initial thermal structure of the upper ocean. The data for both this field and the forecast verification field were obtained from the North Pacific Experiment (NORPAX) TRANSPAC ship-of-opportunity XBT analysis (White and Bernstein, 1979). The geographic location of the gridpoints for these fields are depicted as "X"'s in Fig. 2 and coincide with the Anomaly Dynamics Study (ADS) region (Anomaly Dynamics Study, 1978). The ocean temperatures were obtained by objectively analyzing all the XBT profiles for each month at depths of 0, 20, 40, 60, 80, 100, 120, 150, 200, 300 and 400m. Thus,

fields with an ocean mixed layer model is discussed in Chapter V. A summary of the study, a discussion of the results, and recommendations for the future conclude the thesis in Chapter VI.

Northern Hemisphere atmospheric analysis and prediction system. These surface winds are derived from atmospheric forecast model output and analysis of irregularly scattered observations.

The purpose of this study is to understand the differences and similarities between the SASS and FNOC wind measurements, and the effect that these differences have on ocean mixed layer model forecasts. No study has yet been published comparing the FNOC and SASS wind fields. Therefore, to provide a basis for better explaining model comparison results, a direct comparison of the wind fields will also be made. The inherent weaknesses in both wind fields estimates will be reviewed in light of the results obtained from both direct and model output comparisons.

B. AN OVERVIEW OF THE STUDY

In Chapter II the characteristics of the initialization field, and the FNOC and the SASS boundary conditions used in this study will be described. Also discussed will be the aspects of the SEASAT-A mission which affect the data quality.

The theoretical and practical aspects of the space and time intervals used for comparison of the FNOC and SASS wind fields will be presented in Chapter III. The results of the direct comparisons between the wind fields is presented in Chapter IV. The effect of using the FNOC and SASS wind

have been developed and are being implemented to fill this need.

Synoptic variability in the oceanic mixed layer is largely caused by the local atmospheric wind stress and surface heat fluxes. The accuracy of the wind speed and it's phase with respect to the surface heat flux are critical to correctly model ocean mixed layer deepening and shoaling. Furthermore, the spatial and temporal resolution of the surface forcing data determines the space and time scales which can be resolved with the mixed layer model. The ocean mixed layer model used in this study is a vertically integrated, second order closure parameterization of the turbulent kinetic energy budget (Garwood, 1977). The model is one-dimensional. Therefore, only the heat flux at the surface and the entrainment heat flux at the bottom of the mixed layer can cause changes in the temperature profile at each geographical location. In the model, these individual point profiles are not linked horizontally by any dynamical mechanisms such as Ekman horizontal advection or vertical pumping, or other interior processes. Thus, this study focusses on the impact of the SASS winds on the one-dimensional vertical mixing alone.

For the time period covered by this study, the only other source of wind data over large ocean areas was provided by the Fleet Numerical Oceanography Center (FNOC). This data set consists of surface marine winds from the FNOC

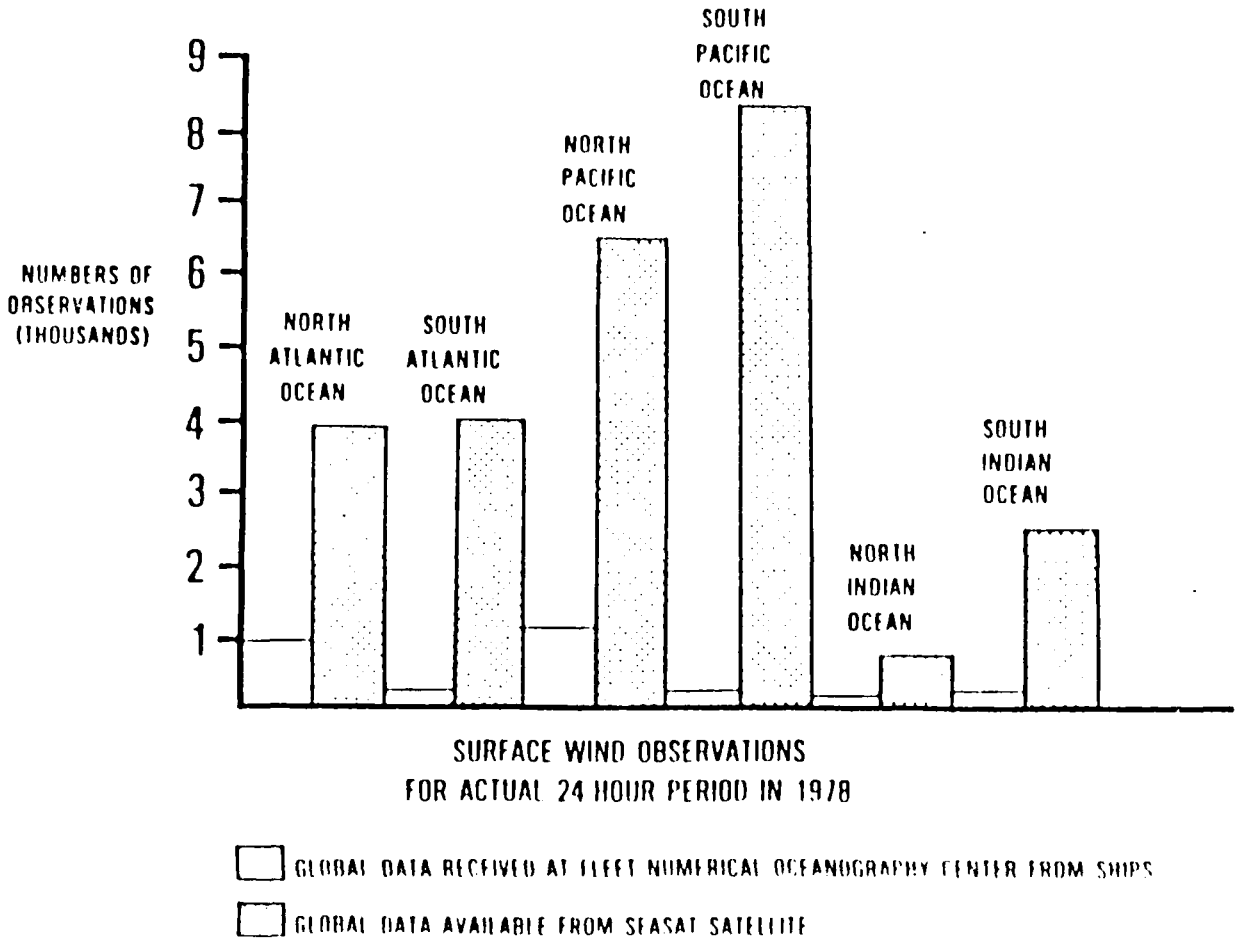

Figure 1. Summary of oceanic surface wind observation densities.

I. INTRODUCTION

A. PURPOSE OF STUDY

This thesis is concerned with the feasibility of using wind measurements sensed by the SEASAT-A Scatterometer (SASS) to derive the surface wind stress boundary conditions for use by an ocean mixed layer model. The SASS wind measurements are a unique source of high spatial resolution data that may provide information important to ocean mixed layer processes on otherwise unavailable time and space scales. In addition to high spatial resolution, the SASS orbital con figuration provided temporal resolution of the order of 36 hours. A comparison of the number of SASS observations and the number of conventional wind observations available for a sample one-day period indicates the potential impact of this data source (Fig. 1). These potential attributes invite investigation into the practicality of using SASS wind measurements to improve ocean model boundary conditions and thus ocean mixed layer prediction capability. The quality, quantity and resolution of the SASS data is addressed with respect to it's potential impact on ocean mixed layer predictions. Although there is not a functional scatterometer currently in orbit, plans

TABLE 2
Summary of SASS Records Eliminated by Quality Control Criterion (4)

Date	Position	Alias Wind Values	AACC	Comment from GOES
22 JUL	49.9N;183.9E	35.6 37.6 ---- ----	Known	In Develop. Low
25 JUL	31.3N;160.9E	27.2 24.4 ---- ----	Unknown	Off Image
27 JUL	43.5N;204.7E	33.0 37.4 ---- ----	Unknown	In Cold Front of Developing Low
27 JUL	42.9N;204.9E	47.2 50.0 ---- ----	Unknown	
27 JUL	42.7N;205.1E	39.8 44.8 ---- ----	Unknown	
27 JUL	38.3N;202.4E	37.0 40.0 ---- ----	Unknown	Partly Cloudy: No Shear Zone Likely
27 JUL	38.2N;201.7E	50.0 50.0 ---- ----	Unknown	
27 JUL	37.7N;200.5E	48.4 46.6 ---- ----	Unknown	
27 JUL	37.3N;200.3E	25.4 29.2 ---- ----	Unknown	
30 JUL	46.3N;182.5E	23.8 26.0 27.2 26.8	Known	In Cold Front
6 AUG	41.7N;194.8E	34.0 32.8 ---- ----	Known	In Polar Low
29 AUG	46.3N;187.1E	29.0 29.6 ---- ----	Unknown	Dense Overcast Clouds, Likely Developing Low
29 AUG	46.5N;186.9E	28.2 28.6 ---- ----	Unknown	
29 AUG	46.4N;187.3E	33.8 34.8 ---- ----	Unknown	
29 AUG	46.6N;187.2E	37.0 38.4 ---- ----	Unknown	

AACC = Antenna Attenuation Correction Coefficient

positioned in regions which were high in atmospheric moisture. The lack of information necessary to make adequate corrections for attenuation of the SASS microwave signal due to atmospheric moisture increases the probability of these high wind speeds being erroneous. There is no means by which they can be definitively proven to be correct. All three of the measurements with a known AACC covered regions very likely to have had wind shear zones associatated with fronts or storm activity. These three measurements were not reinforced by other coincident measurements with similar values. The record for the 22nd of July was coincident with (within 0.5 degrees latitude or longitude and within 24 hours) 14 other records (all having a known AACC) with an average wind speed of 10.2 m/s. The record for the 30th of July was coincident with eight other records (all with a known AACC) having an average wind speed of 15.2 m/s. The record for the 6th of August was coincident with eight other records (3 with a known AACC), all averaging 16.6 m/s. The lack of coincident points to justify the 25 m/s values demonstrates the need to impose criterion (4), despite it's somewhat ad hoc nature.

Imposing these four additional quality control criteria eliminated 76,104 (28 %) of the data records. It is believed that the screened SASS data set contains the highest quality data which can be derived from the SASS data record for this time period.

III. RESOLUTION

A. BACKGROUND

The desired resolution for any numerical model is determined by the physical processes that it is designed to simulate. Determining whether or not these desires can be met is a fundamental step in analyzing the usefulness of available data sets. In this study, spatial scales of the ocean mixed layer model are already restricted by the temperature field (White and Bernstein, 1978) used to initialize and verify the model. Therefore, spatial scales of 2 degrees latitude by 5 degrees longitude are determined by the minimum requirements to be met by the data sets supplying the wind forcing boundary condition.

The temporal resolution of an ocean mixed layer model is limited by the temporal resolution of the model's boundary condition data sets. The FNOC analyses has wind speed values every six hours, which allows temporal resolution of waves 24 hours long. The data are spline interpolated to intervals of one hour to provide model stability, though maintaining a 24-hour resolution of geophysical events. Thus the diurnal cycle is the shortest period phenomenon resolvable with the FNOC data.

The spatial resolution of the SASS data set was examined first. Then the temporal resolution of the data had to be determined so that a comparison grid reasonable for both FNOC and SASS data sets could be defined.

This chapter will review the theoretical scales of the dynamic and thermodynamic processes important to ocean mixed layer predictions. Next, a brief summary of the FNOC wind data resolution is presented. Then, a more detailed survey of the SASS data resolution characteristics is given. Finally, the comparison grid used for the remainder of the study is defined.

B. THEORETICAL SCALES OF MOTION

Momentum, mass and heat fluxes through the ocean surface are responsible for many of the motions of the ocean. Atmospheric pressure variations and winds produce momentum fluxes across the air-sea interface causing turbulence, currents, and various types of wave motion.

A lag in the ocean's response to atmospheric fluctuations is caused by its relatively high inertia. This factor further complicates the understanding of air-sea interactions, since the oceanic response is rarely in equilibrium with the changing atmospheric conditions. The lag important to mixed layer processes ranges from hours, associated with oceanic (inertial) motions and atmospheric

diurnal fluctuations, to months, associated with atmospheric seasonal changes.

The relatively high inertia of the ocean affects the spatial scales as well. For example, the scale of synoptic eddies is proportional to the Rossby radius of deformation. In the atmosphere this scale is of the order of 1000 km and can be resolved with a grid spacing of 250 km. However, in the ocean, the Rossby radius of deformation is of the order of 100 km and therefore oceanic mesoscale eddies are resolved only with a grid spacing of 25 km or less.

There are four main scales of atmospheric forcing events which are associated with various oceanic scales of motion. The first includes seasonal atmospheric variations on the spatial scale of ocean basins.

On this scale the ocean responds to the atmospheric zonal wind and meridional changes in the atmospheric temperature gradient. These responses are in the form of Ekman pumping/suction, horizontal advection of water masses by ocean gyres and changes in the seasonal mixed layer depth.

The second scale is the atmospheric synoptic scale which encompasses spatial variations of the order of 1000 km and temporal fluctuations ranging from one to ten days. The ocean responds to forcing at this scale with changes in the mixed layer stability and depth, and formation of ocean fronts.

The third scale is the atmospheric mesoscale, which is associated with storm fronts, polar lows, and hurricanes. These events take place at temporal scales of the order of hours, and spatial scales ranging from 10 to 100 km. The ocean's response at this scale includes turbulent storm mixing and inertia-gravity wave formation.

The fourth scale is the diurnal scale produced by the daily variation in solar radiation at the sea surface. Thermodynamic responses to atmospheric forcing warm (cool) the ocean's upper layers. This increases (decreases) the hydrostatic stability, which dampens (enhances) the effect of turbulent wind mixing. The temporal scale is fixed at 24 hours. The relevent spatial scale is vertical rather than horizontal; it is the Obukov depth scale, which is determined from the ratio of shear production to bouyancy flux into the layer. The diurnal cycle is emphasized as a separate atmospheric forcing scale because it primarily affects ocean mixed layer thermodynamics. The ocean mixed layer's response to the diurnal scale forcing may be viewed as changes in available potential energy. Radiative cooling at night causes convective mixing, which lowers the available potential energy and deepens the mixed layer. Warming of the photic zone during the day raises the mixed layer's available potential energy and increases the layer's stability, inhibiting turbulent mixing by the wind.

C. RESOLUTION CHARACTERISTICS OF THE FNOC DATA SET

As noted in Chapter II, the temporal scale of the FNOC wind data set used for this study is 6 hours. This is sufficient to resolve the ocean mixed layer's response to the atmospheric diurnal cycle.

The spatial resolution of the FNOC data is determined by the grid used for the atmospheric model. The grid is a 63 by 63 polar stereographic projection of the Northern Hemisphere, true at 60N. Because of the projection, the spatial resolution changes with latitude. The scale, however, is clearly synoptic, and varies from 306km at 30N to 360km at 50N. The ocean thermal structure field has a 2 degree latitude by 5 degree longitude spatial resolution (approximately 240km by 600km). Thus, the FNOC wind fields have a finer spatial resolution than the ocean thermal structure fields in the zonal direction, but a coarser resolution in the meridional direction. Therefore, when the FNOC winds are used as a boundary condition, the model spatial resolution is limited by the ocean thermal structure fields in the zonal direction and by the wind fields in the meridional direction.

D. RESOLUTION CHARACTERISTICS OF THE SASS DATA SET

It is important to establish an initial overview of the characteristics of the SASS data coverage. Reasonable choices must be made in determining a spatial grid scale and

time interval useful both for comparison with the FNOC data fields and for specifying mixed layer model boundary conditions.

1. Spatial Coverage

The geometry of the SEASAT orbit, the effects of the earth's rotation, and the variations in instrument operating mode each contributed to SASS's characteristic spatial coverage. While the coverage aspects due to orbital geometry and earth's rotation were predictable, the fluctuations in coverage produced by changes is SASS operating modes were random. The following sections outline the results and implications of the effect that each of these three main aspects had on spatial coverage.

a. The Geometry of the SEASAT Orbit

SEASAT precessed about 26 degrees of longitude every orbit or 365 degrees of longitude every day. Its surface coverage resulted in a criss-crossing pattern of orbital paths (Fig. 3). This pattern reveals the inherent dependence of spatial resolution on latitude. There is an increase in data density due to satellite swath intersections, both between ascending and descending tracks and also where convergent tracks overlap as the poles are approached. The impact of latitudinal dependence on spatial coverage variations, though predictable, is a primary concern in resolution considerations. Also, the daily precession of the SEASAT orbit by 5 degrees longitude beyond

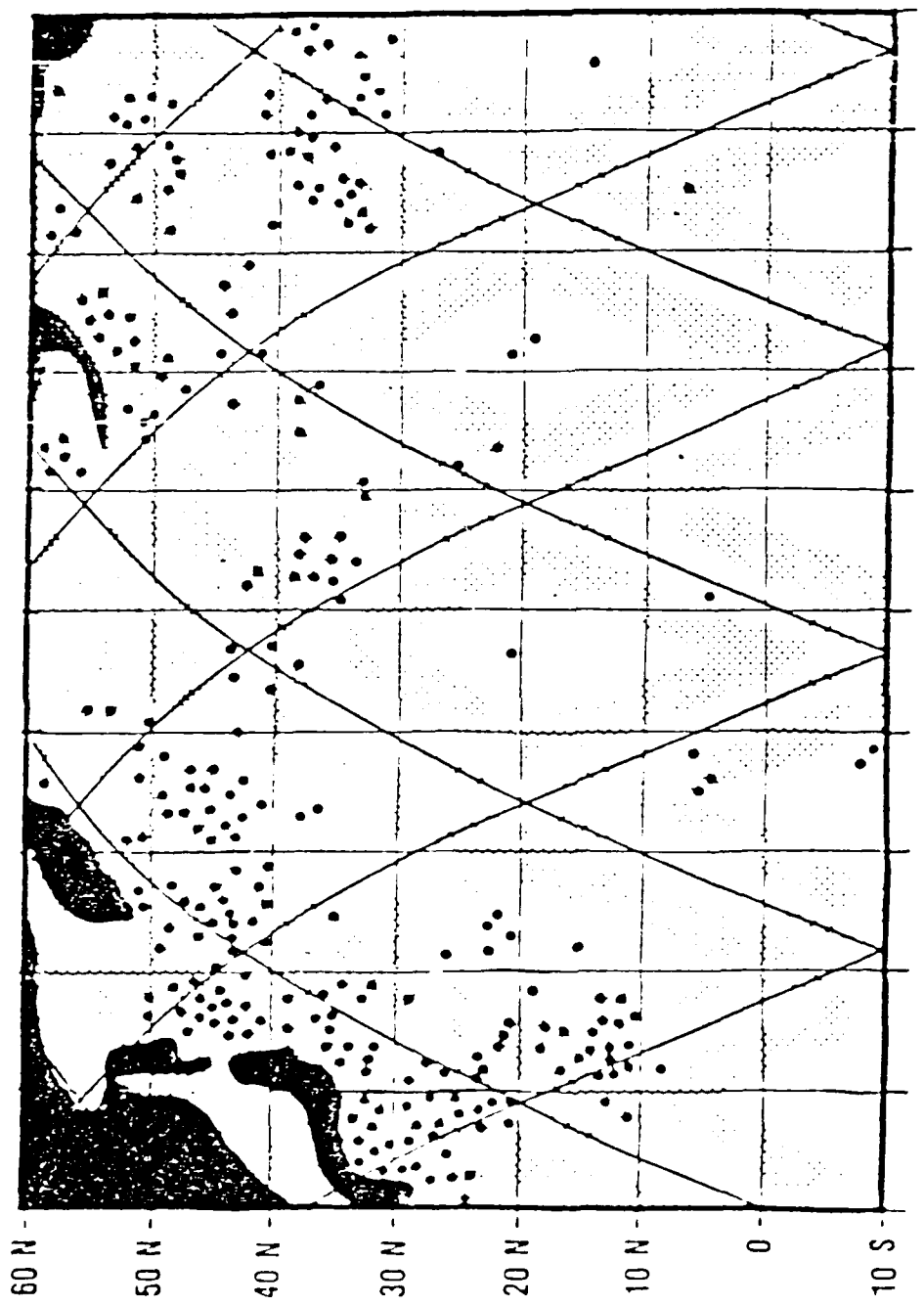

Figure 3. The coverage pattern of SASS during the 14 orbits of a 24 hour period while sensing in a double swath mode as compared with conventional observation distribution.

its previous nadir path yielded a negligible variation in data coverage across the study area.

b. The Effect of the Earth's Rotation

As the earth rotates, it's movement alters the doppler frequency shift employed by SASS to track the geodetic position of its measurements. Because the antennas have a fixed frequency range, the width of the swaths covered by the forward antenna is different from that covered by the aft antenna. The antenna that was able to receive the widest swath depended upon the direction of the satellite. The forward antenna swath is widest when descending, and the aft swath is widest when ascending. Table 3 shows typical values for the variation incurred by this effect. A wind speed cannot be determined unless the ground area sensed from the fore and aft antennas overlap. Hence, the narrowest swath will determine the width of data coverage (Fig. 4). This variation will cause a net increase in ground data density with increasing latitude because the narrowest swath is wider at higher latitudes. The higher the latitude, the wider the swath and the fewer number of orbits needed to cover the area.

c. The SASS Operational Modes

This effect stemmed directly from the various data gathering modes in which the scatterometer operated. Each mode was produced using various combinations of horizontal and vertical polarization with each of the four

TABLE 3
SASS Swath Width Variations at Selected Latitudes

Latitude (N) (degrees)	Swath Width (km)			
	Right Front	Right Aft	Left Front	Left Aft
72 (A or D)	625	625	625	625
40 (A)	720	508	720	508
0 (A)	785	490	785	490
40 (D)	508	720	508	720
0 (D)	490	785	490	785

A = Ascending; D = Descending

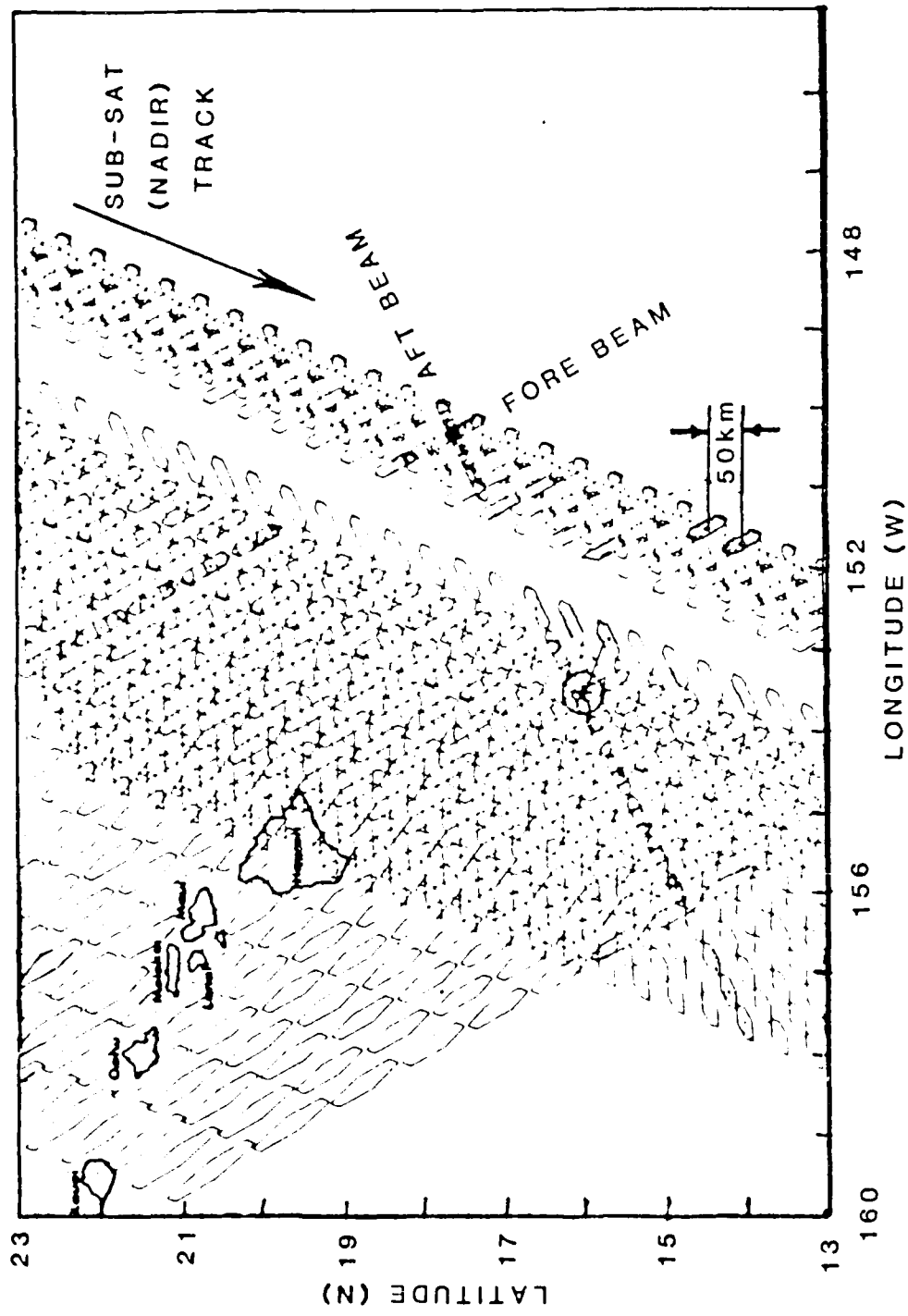

Figure 4. The pattern of fore and aft antenna beams. An illustration of the SASS swath distortion because of earth's rotation. Only the area sensed by both fore and aft antennas yielded wind vector solutions.

antenna sticks (See Table 4). This enabled coverage on either the left or right sides of the satellite's path in six modes or on both sides of nadir at once in two modes. When SASS was operating so that only a single side was being sensed, the data coverage was twice as dense as when both sides were being sensed. The width of side swaths (Table 3) didn't change for various modes. The nadir swath nad an average width of 140 km when both side swaths were being sensed and 90 km when only one side swath was being sensed. A gap of 110 km separated the side swaths from the nadir swath in all modes.

d. The Summary of SASS Spatial Coverage Characteristics

As an aid to this summary, the variations in spatial coverage that result from many of the effects discussed above are illustrated in Fig. 5a and b. The spatial bin size contoured is 1 degree by 1 degree.

The time increment for each "frame" in Fig. 5a is 101 minutes (the time required for one satellite orbit). Only eight of the 14 time frames for this day are shown. The remaining 6 contained no data because the orbit path fell outside the study region. As expected, the sensor's spatial coverage, though generally predictable, does not nave a consistent data density.

In Fig. 5b, the result of combining the individual orbit passes for a single day is seen. Although

TABLE 4
SASS Operational Mode Descriptions

Mode	Polarization	Antenna Switching Sequence
1	Verical	4 (LF), 1 (RF), 3 (LA), 2 (RA)
2	Horizontal	4, 1, 3, 2
3	Mixed	4 V, 4 H, 3 V, 3 H
4	Mixed	1 V, 1 H, 2 V, 2 H
5	Vertical	4, 4, 3, 3
6	Vertical	1, 1, 2, 2
7	Horizontal	4, 4, 3, 3
8	Horizontal	1, 1, 2, 2
9		Calibration
10		Standby

L = LEFT, R = RIGHT, A = AFT, F = FORWARD
H = HORIZONTAL, V = VERTICAL

"*"s in Fig. 2. The records for each bin were then averaged to obtain a single wind speed value for each 24-hour period. These steps yielded a 10 by 14 grid of data every 24 hours for 34 days. For each 24-hour time frame this grid of data was then interpolated, using a two-dimensional fifth order polynomial, onto a similar grid, designated by "O"'s in Fig. 2. This was done to coincide with the ADS grid points used for later model simulation. The products of this interpolation step were fields on a 9 by 13 grid, every 24 hours for 34 days. The interpolated grid was truncated to the reduced ADS grid (Fig. 2), resulting in a 6 by 12 data matrix for each of the 34 days.

3. Interpolation of FNOC Data onto Comparison Grid

The six-hourly FNOC fields were linearly averaged in time for each 24 hour period, centered at 1200Z. The data set was truncated in time to a 34 day period beginning July 15, 1978, and ending August 18, 1978. The spatial coverage was then truncated from the ADS grid to the reduced ADS grid (Fig. 2).

As with SASS fields, the result was a data file containing 34 daily grids, each dimensioned 6 by 12 and covering the reduced ADS grid area.

NORPAX ADS ocean temperature analyses previously used to initalize and verify Garwood's model (Gallacher, et al. 1983) and in the meridional direction by the Northern Hemisphere grid employed by FNOC at the time of the creation of the data base, interpolated onto even degrees of latitude.

1. Boundaries of the Comparison Grid

The comparison grid dimensions are chosen to correspond to a subset of the ADS grid (designated as the "reduced ADS grid") which has been used for previous studies (Gallacher et al., 1983). There were two reasons for choosing the reduced ADS grid over the ADS grid for direct and model comparison of the FNOC and SASS fields:

(1) the reduced grid may minimize horizontal advective effects induced in the temperature field by the Kuroshio Current extension;

(2) areas of sparse ocean data density in the ADS region are avoided.

2. Interpolation of SASS Data onto Comparison Grid

The SASS data set was truncated in time to cover a 34 day period from July 16, 1978 through August 18, 1978. This particular time frame was chosen to span two consecutive mid-month analyses of the upper ocean thermal structure field as documented by White and Bernstein (1979).

The data records for each 24 hour period (centered on 1200Z) were sorted into 2 degree latitude by 5 degree longitude bins. The centers of these bins are depicted by

IV. DIRECT COMPARISON OF DATA SETS

A. GENERAL

Using the results of Chapter III, a grid was chosen to compare the SASS and FNOC wind fields. The first section of this chapter reviews the description of the comparison grid and the method of reducing the SASS and FNOC data sets onto it. Next the methods and results of a direct comparison of the FNOC and SASS data fields are presented. These comparisons provide initial insight into the similarities and differences of the fields, and they provide a basis to better interpret later ocean model comparisons.

B. THE COMPARISON GRID

The fields are resolved on identical 2 degree latitude by 5 degree longitude grids. The time interval for both fields is 24 hours. These space and time scales are a compromise between the possible temporal resolution in the FNOC data and possible spatial resolution in the SASS data which allows the data bases to be sufficiently complete for initial comparison. A temporal dimension of 24 hours was chosen, over the FNOC dimension of six hours, to avoid large spatial gaps in the SASS data. The spatial dimensions were limited in the zonal direction by the resolution of the

by the SASS wind fields and on spatial scales by the initialization fields.

The resolution of FNOC wind fields is defined by the atmospheric model used to compute them. The horizontal spatial scale is of the order of 300km. This will allow resolution of atmospheric forcing events with a wavelength of 1200km. The temporal scale of the FNOC wind data is 6 hours, allowing resolution of diurnal forcing fluctuations.

The SASS wind field resolution is defined by instrument parameters and orbital configuration. The horizontal spatial scale is 50km, enabling resolution of mesoscale events with fluctuation wavelengths as small as 200km. The temporal resolution of the SASS fields is irregular because of sporadic changes in operational modes. However, the scale is of the order of 24 hours. This scale is able to resolve fluctuations in atmospheric forcing events with periods of 4 days.

These results show that the model has a spatial resolution limited by the oceanic thermal structure initialization field. The FNOC and SASS wind fields have finer resolution available, with the SASS fields holding the highest potential in this aspect. Additionally, operation by SASS in modes that enable a continuous double swath coverage could reduce the temporal resolution of the SASS fields to a 12 hour scale. Even so, the FNOC wind fields have the highest temporal resolution. Therefore, the model resolution used for comparison is limited on temporal scales

the seasonal thermocline as well as definition of the synoptic mixed layer depth.

The spatial resolution of the heat flux boundary condition fields are on the atmospheric synoptic scale because they have been derived from climatological data which is able to define SST gradient with scales of the order 600km. Although, the original spatial resolution of the fields developed by Wyrtki (1965) were 2 degrees by 2 degrees, they were published with a resolution of 10 degrees by 10 degrees. The coarser resolution was used for this study. The synoptic heat flux variations resolved by these fields provided forcing that did not restrict model resolution for the particular study region and period used. The climatological heat flux fields used had a time scale of one month. Garwood (1977) showed the importance of resolving the diurnal cycle with the heat flux fields to ocean mixed layer model dynamics. To provide this resolution, a prediction of the diurnal cycle associated with the radiative heat flux was superimposed on the total heat flux field using a sinusoidal curve fit which was a function of latitude, julian day and hour of the day. The temporal resolution of the heat flux fields is able to define the diurnal cycle. This temporal resolution was made possible by application of theoretical considerations of the diurnal heat budget.

E. RESULTS AND DISCUSSION

The resolution characteristics of the mixed layer model initialization and boundary condition fields, as well as the those scales of motion theoretically important to mixed layer modeling have been reviewed.

The initalization field has horizontal spatial scales of about 240km meridionally by 600km zonally. These scales will resolve ocean temperature fluctuations with wavelengths of motion of the order of 1000km in the meridional direction and 2500km in the zonal direction. Therefore, the initalization field is able to resolve only ocean events which occur on the atmospheric synoptic scale or larger. These events include mixed layer depth fluctuations due to Ekman pumping, horizontal advection of water masses by ocean gyres and features 1000km or more in width. These horizontal scales can also resolve the length of ocean fronts, although not their width. The dominant oceanic horizontal temperature gradient on these scales is meridional. This is also the direction of the finest horizontal resolution, enabling the best available definition of the most important ocean thermal structure characteristics. The vertical scales of the initialization field enable resolution of fluctuations with wavelengths of 80m in the upper 120m of the mixed layer and wavelengths of 100m below 120m. These vertical scales enable resolution of

The advantage of using an interpolation scheme to fill grids with less than 100 per cent coverage rather than decrease temporal resolution accordingly is well demonstrated by these results. Although these percentage calculations are rough averages, nearly a doubling of the number of orbits (or halving of temporal resolution) is required to increase the percentage of area covered from 90% to 100%. The disadvantages of using an interpolation routine to allow an increase in temporal resolution stem primarily from the probable error of estimating a "best guess" value where measured values are desired. The effects of the interpolation scheme on the SASS data fields will be discussed in a later section.

Since the 2 degree by 5 degree spatial bin dimensions are the limits imposed by the ocean temperature fields used by Garwood's model, these results are of particular interest. The use of these spatial dimensions requires a temporal period of 15.3 orbits (slightly longer than 24 hours) for an area coverage of 70%. These time-space dimensions are acceptable for model use and provide adequate coverage for interpolation requirements.

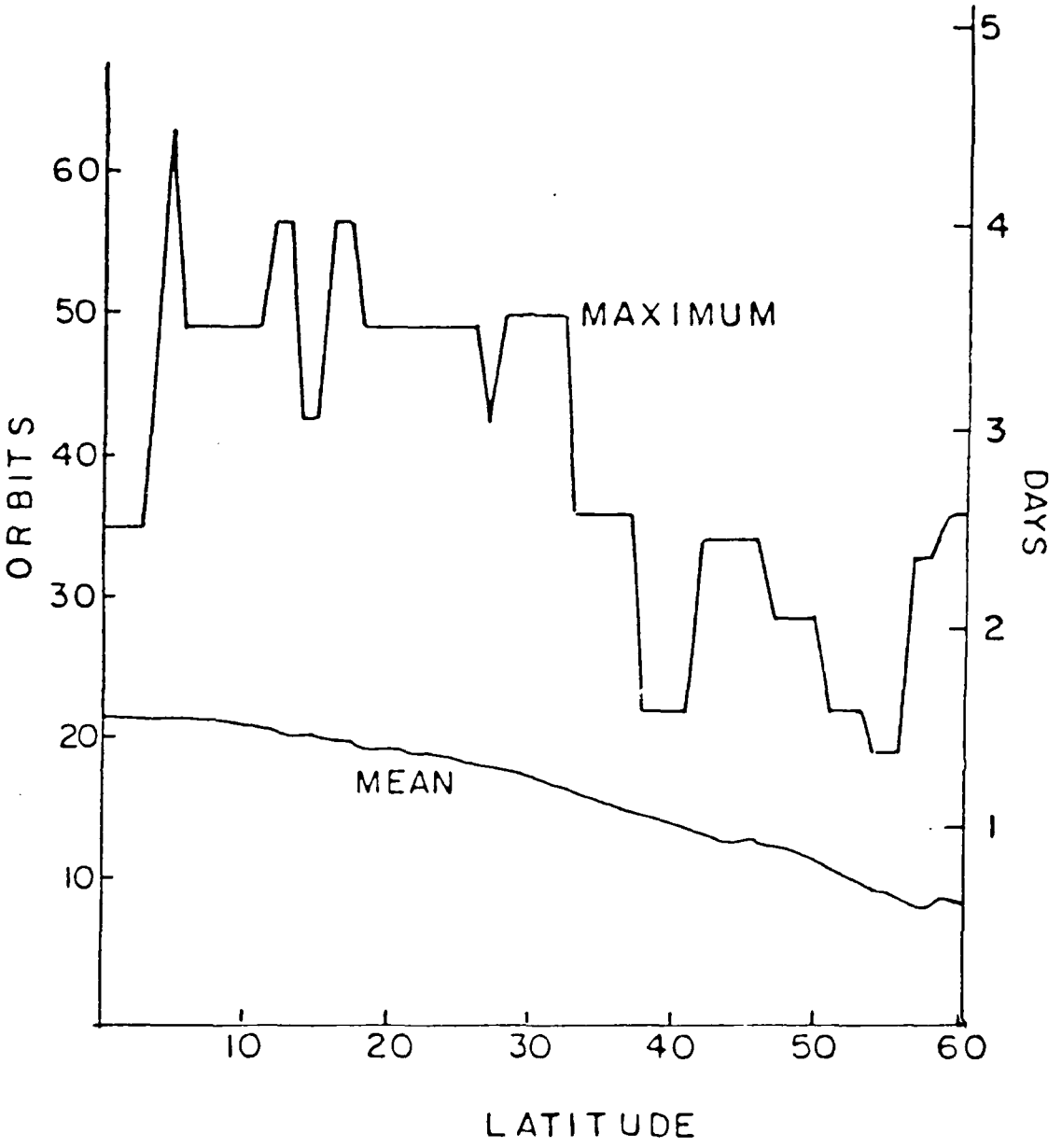

Figure 6. Variation in SASS temporal resolution with latitude. The mean and maximum time required for SASS to re-sense a nadir point varies with latitude.

a. Revisit Time

The time between successive samples of wind at a single ground point is defined as "revisit time". This quantity assumes the instrument operated in a double swath mode and is graphed in Fig. 6 based on predictable coverage characteristics.

The interrelationship between spatial and temporal coverage is seen by comparing Fig. 3 and Fig. 6. The intersection of orbit passes seen in Fig. 3 is related to the maximum time required for a revisit as shown in Fig. 6. The mean values of revisit time in Fig. 6 may be attributed to the variation of swath width with latitude.

b. Dependence of Temporal Resolution on Spatial Coverage

Since the study area cannot be viewed as a single point for temporal resolution considerations, the interrelationship between spatial coverage and temporal resolution was examined.

The average number of orbits (measured from three randomly selected start times) required to cover the following percentage of the study area for fixed spatial bin dimensions of 2 degrees latitude by 5 degrees longitude was calculated. The results are:

70% coverage requires 15.3 orbits,
80% coverage requires 17.6 orbits,
90% coverage requires 20.0 orbits,
100% coverage requires 41.6 orbits.

sided swath (mode 4,6 or 8). This is apparent from the lack of data on the left side of the subtrack and from the doubling of data density on the right side of the subtrack. The subtrack in each frame is bordered by data gaps which make it distinguishable.

The data coverage for each of the remaining frames may be explained in a similar manner. The inconsistencies in coverage imposed by hundreds of relatively rapid operational mode changes (of the order of 5 minutes in duration) every day are the primary cause of sporadic data distribution. The SASS data set may be considered as a "worst case scenario" in terms of spatial coverage, since the SEASAT mission was aborted long before long-term coverage in any one operational mode could be maintained.

From this illustration, it becomes clear that the SASS data contain adequate spatial coverage to be used to define the boundary conditions for Garwood's mixed layer model.

2. Temporal Resolution

Having determined that there is adequate spatial coverage for an ocean mixed layer model, the temporal resolution was examined. The best time scale available for comparison of the wind fields was sought.

the exact spatial coverage cannot be predicted for a given day because of the random changes in operational mode, the general character is illustrated by this figure.

The SEASAT orbital pattern created a dependence of spatial coverage on latitude. This is seen in both Fig. 5a and 5b by noting the latitudes where various paths intersect or form gaps. Also, the precession of the orbit, shown in Fig. 5b, provides excellent spatial coverage as long as the operational mode designated allows swaths to be sensed on both sides of the nadir path at once. The effects of the earth's rotation on spatial coverage are negligible over the study region.

Examination of the SASS data set used in this study reveals that spatial coverage for time frames of the order of one day or less contain unsystematically large data-void regions approximately 10 per cent of the time. These regions are oriented north-south and usually extend to the borders of the study area. The unpredictable character of the coverage is directly attributable to the continual changes in the SASS operational mode.

Evidence of the different operational modes activated over the course of a single day is shown in Fig. 5a. Frame 6 of Fig. 5a shows an ascending orbit which enters the area in operational mode 1 or 2 (sensor swaths on both sides of the satellite nadir swath). Part way through the frame, the operational mode was switched to a right

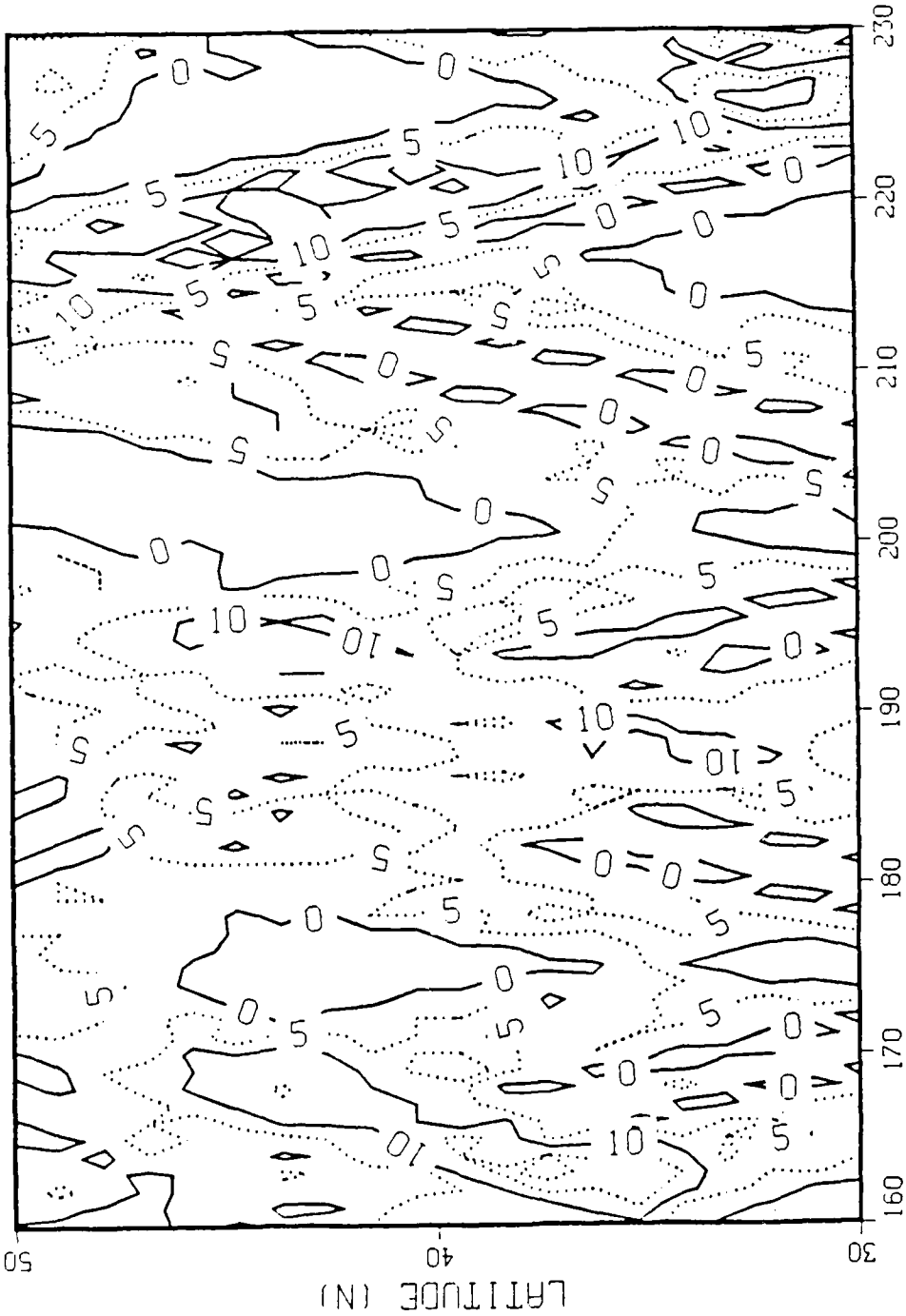

Figure 5(b). Spatial distribution of SASS data for a single day. The result of overlaying orbital frames shown in Fig. 5(a).

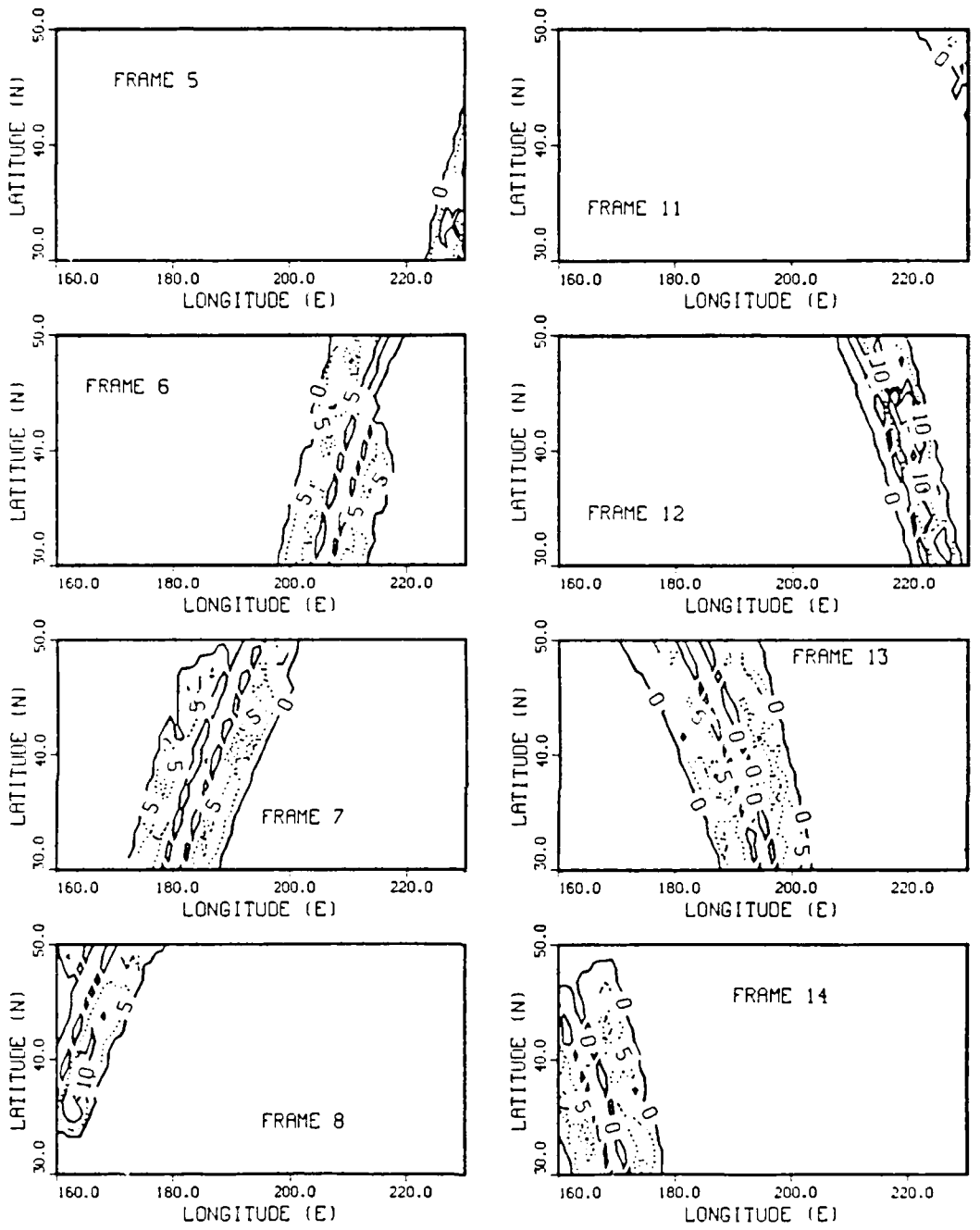

Figure 5(a). SASS data density per 1 degree by 1 degree bin for each orbit during August 3, 1978. Orbital frames 1,2,3,4,9 and 10 contained no data and are ommitted. CI = 5, alternating solid and dotted with 0 solid.

C. COMPARISON OF WIND FIELD CHARACTERISTICS

1. The Spatial Means

The spatial mean was computed for each 24-hour grid for both FNOC and SASS data sets. The resulting time series of spatial means is presented in Fig. 7a. The time series begins with July 15th, 1978 as Day 1.

No consistently strong bias in wind speed values is evident in the time series. In general, the correlation between field means is good, indicating no detectable phase shift between data sets. Although the time resolution of one day is rather coarse, this characteristic is promising because it ensures that the same model interaction between the momentum and bouyancy flux boundary conditions is maintained regardless of whether the FNOC or the SASS wind field is used. Although the spatial means show generally good agreement, there is a period of 7 days starting on day 6 and a period of 4 days starting on day 15 for which the SASS means are consistently higher than the FNOC winds. Conversely, there is a 4 day period starting with day 20 for which the FNOC winds are consistently higher. These seemingly minor variations (of the order of 1 m/s) in the means may, however, be significant for the mixed layer model. This will be discussed in detail in Chapter V.

2. The Spatial Standard Deviations

Fig. 7b shows the standard deviation for each field associated with the means in Fig. 7a. As with the means, no consistently strong bias appears in these values. Thus, the SASS and FNOC fields agree not only in the average magnitude of the wind measurements, but also in overall spatial variation, though not necessarily in spatial patterns. This agreement between the overall variance of the fields is an important factor in the prediction of surface wind stress, since the stress is proportional to the square of the wind speed.

3. Isotach Contours

Having determined that the means and standard deviations are in good agreement, a comparison between the isotach patterns of each wind field was made. For modeling ocean mixed layer responses to mesoscale atmospheric events, the horizontal variation of the wind stress is at least as important as the average and the variance of the wind stress. Fig. 8 presents a comparison of the percent coverage of the SASS data field before interpolation, the pattern correlation between SASS and FNOC isotach contours and the root mean square (RMS) error between the SASS and FNOC fields.

The coverage of the SASS data was always above 55%, where 100% denotes no data gaps for that day. The average coverage was 86%. As discussed earlier, the coverage has no

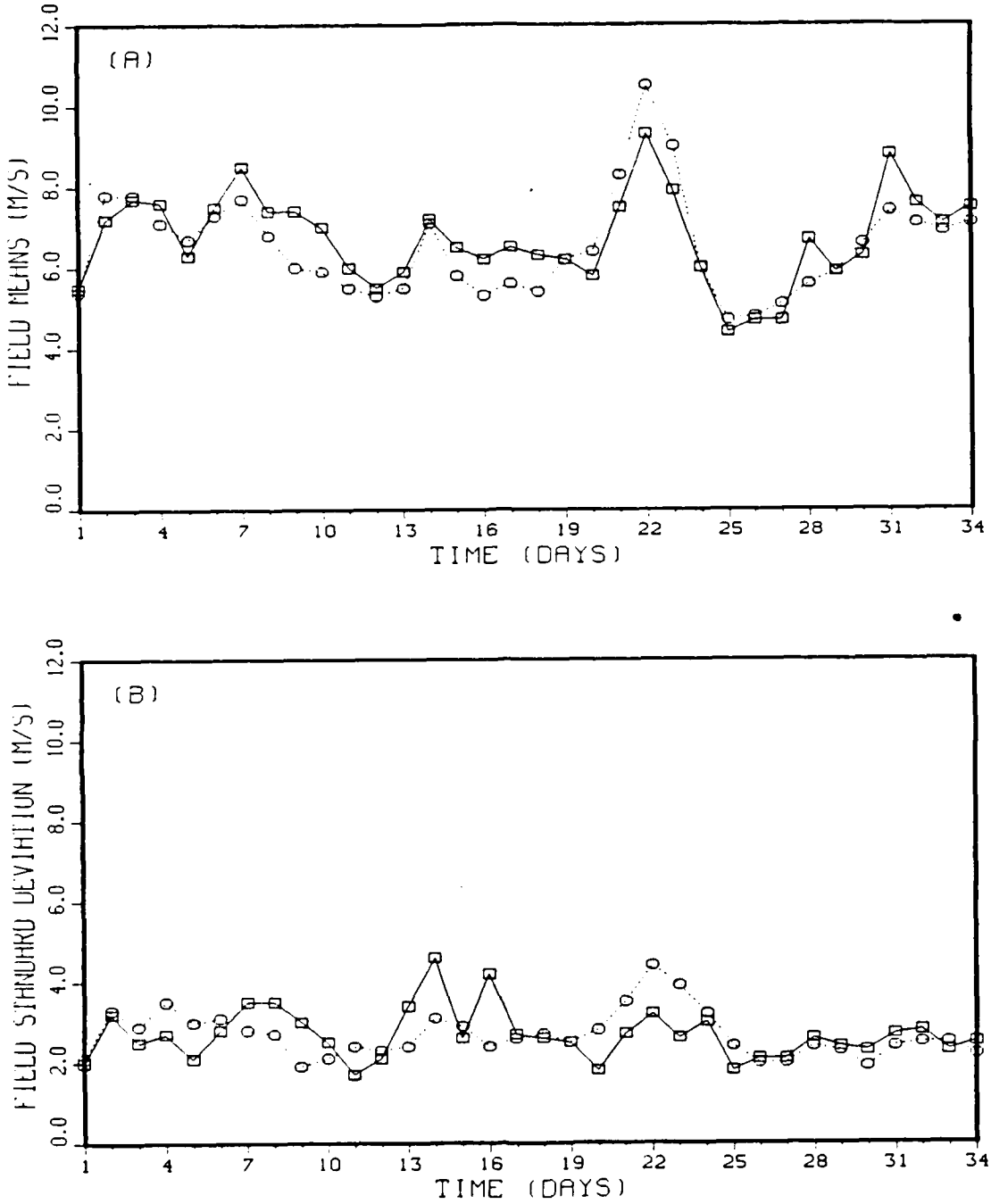

Figure 7. (a) Comparison of SASS (solid) and FNOC (dotted) field mean time series.
(b) Same as (a) for standard deviation.

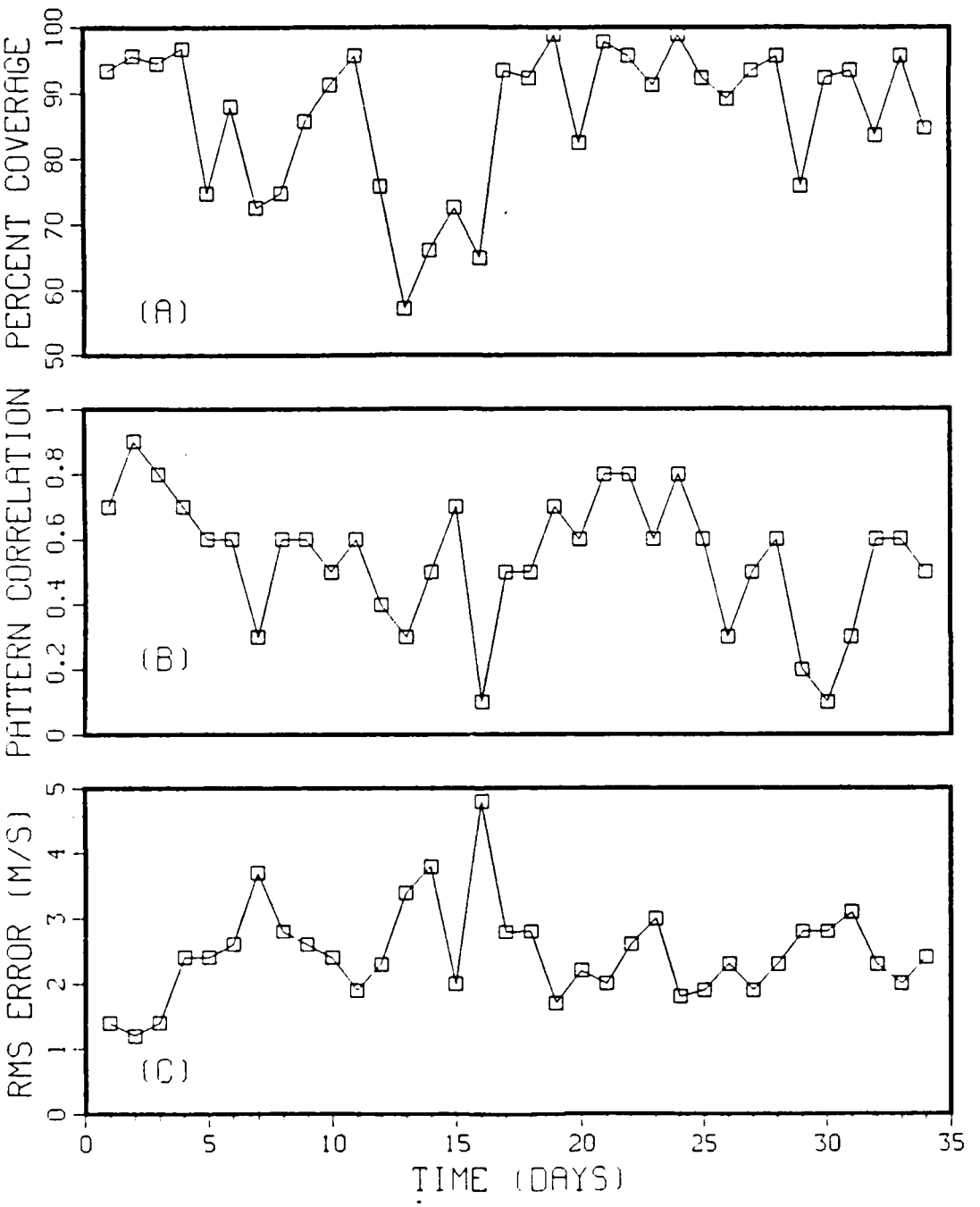

Figure 8. Time series: (a) Percent coverage of SASS data before interpolation. (b) Pattern correlation between SASS and FNOC isotach analyses. (c) RMS error between SASS and FNOC isotach analyses.

predictable pattern for individual days. The pattern correlation between FNOC and SASS fields shows very high correlation between the fields for most days. The pattern correlation plot is mirrored by the RMS error plot.

There is a strong similarity between the graphs of percentage of the area covered by SASS data and the pattern correlation between SASS and FNOC. This similarity suggests that the difference in the isotach patterns on those days is related to data gaps in the SASS data field before interpolation. Where the coverage percentage is high, the pattern correlation and RMS error show very good agreement between the SASS and FNOC fields.

It should be stressed that these contours are isotachs and not streamlines. The scale of variation for wind speed is considerably smaller than for wind direction, making a high correlation between isotachs more difficult to achieve than for streamlines.

4. The Extremes of Correlation

A brief comparison of the data density contours and the isotach patterns for the days with the best and worst correlation was made. This was done to determine, in a qualitative sense, the conditions that contribute to the quality of the two data sets. Sea surface pressure analyses revealed the synoptic patterns associated with the FNOC isotach patterns. GOES satellite imagery was used as an

independent data source to verify synoptic events influencing both SASS and FNOC isotach analyses.

The Appendix stresses the results for all 34 days used in this study, similar to Figs. 9 and 10, which will be presented in the following sections. This allows a complete review of the details of both SASS and FNOC data sets.

a. The Best Case

Day 2 (July 17, 1978) was chosen from Fig. 8 as the day on which the data fields compared most favorably. Fig. 9 presents the SASS data density contours and isotach analyses for both SASS and FNOC.

The SASS data density (Fig. 9a) is consistently high over the study region. The only regions of zero coverage are two narrow areas extending from the northern border of the ADS region through 40N and centered zonally at 174E and 199E. The agreement between the SASS and FNOC wind speed fields (Fig. 9b and c) is very good and illustrates the potential reliability of the scatterometer for measuring wind speeds over large areas. The GOES satellite imagery for Day 2, compared well with both the FNOC and the SASS fields. This imagery indicated the presence of an occluded low pressure system centered at 49N and 167W, which accounts for the isotach pattern associated with the maximum wind speed region dominating Fig. 9b and c. Also, the FNOC surface pressure chart for that day verifies the presence of the low and shows two high pressure systems, one in the northeast

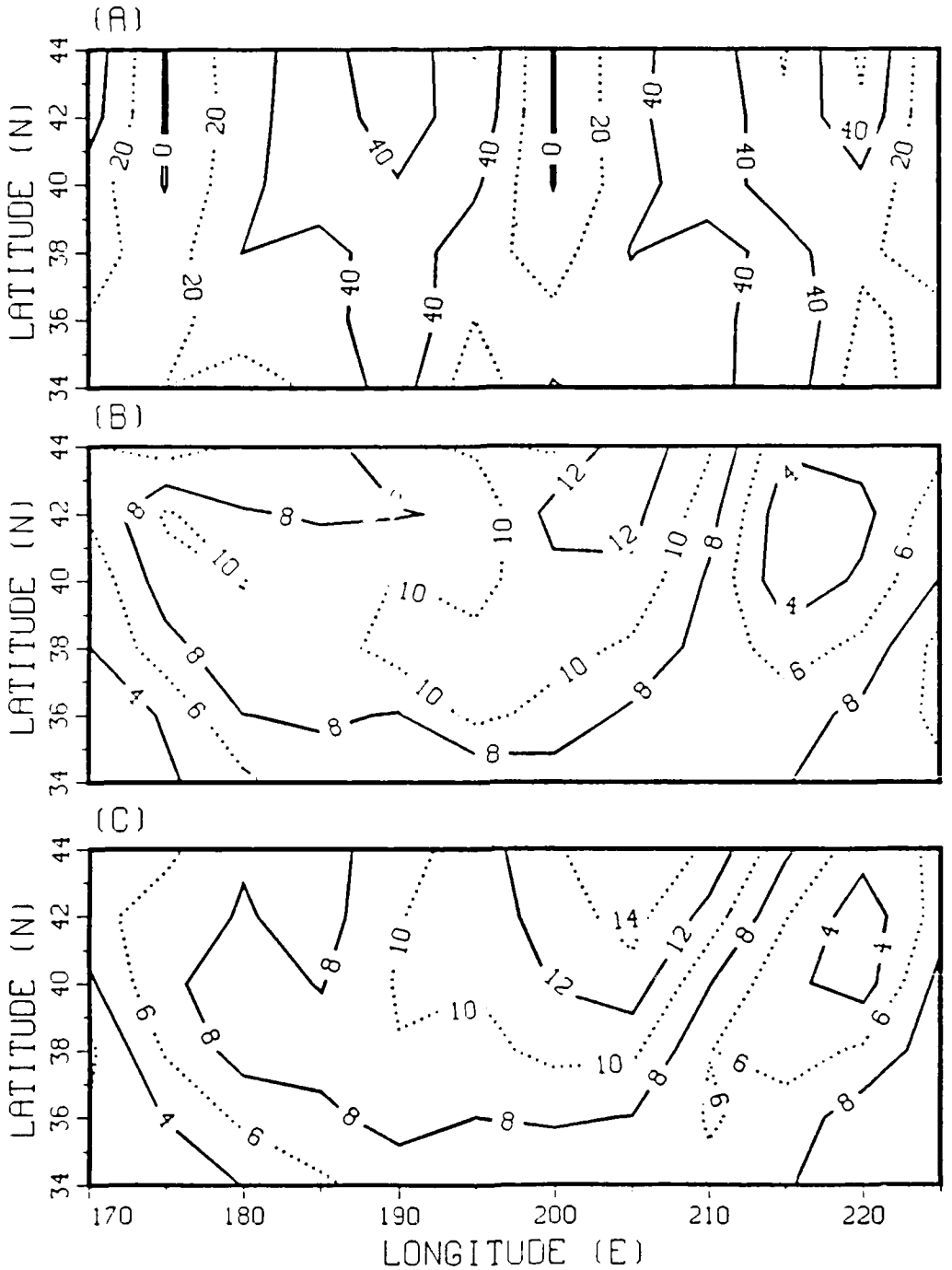

Figure 9. (a) SASS data density; July 16, 1978 (Day 2). CI = 5, alternating solid and dotted with 0 solid. (b) SASS isotach analysis; same day. CI = 2, format as is (a). (c) Same as (b) for FNOC data.

corner of the study region and the other in the southwest corner. Of particular interest for modeling is the agreement between the magnitude of the wind speed gradients for the two fields.

Although the agreement is very good, some differences are apparent The FNOC isotach analysis appears to be shifted east three or four degrees longitude relative to the SASS analysis. The position error is most likely due to the use of a model to predict the 6-hourly FNOC winds. The model relies on a widely scattered distribution of data for its initial conditions, whereas SASS provides direct observations with negligible position errors. The differences between the fields are so slight that neither may be considered in error without corroborating ground truth measurements, which do not exist.

b. The Worst Case

Day 16 (July 31, 1978) was chosen from Fig. 8 as the day on which the data fields compared least favorably. Fig. 10 is the same as Fig. 9, except for Day 16.

The SASS data density contours shown in Fig. 10a illustrate the pattern that is characteristic of days with many data gaps. The data density is not consistent and it has sharp maxima and minima. The data gaps are large and extend to the study region borders. The dominant gradients on the atmospheric synoptic scale are in

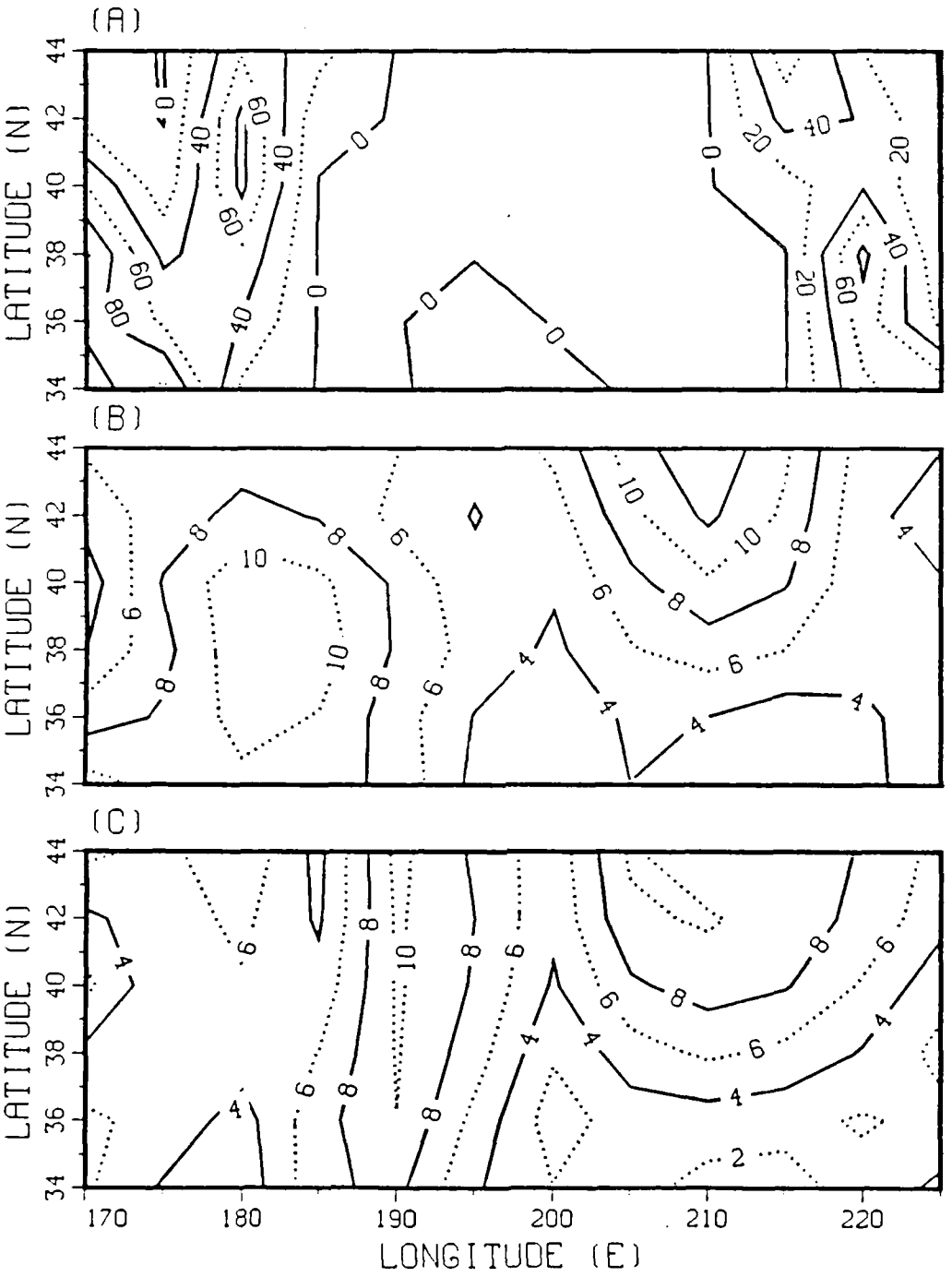

Figure 10. Same as Fig. 9, except for July 30, 1978 (Day 16).

the meridional direction. Since mesoscale atmospheric events also contain strong zonal gradients, the orientation of these data gaps is an important factor in the capability to fill gaps accurately by interpolation. This factor will be discussed further in the following section. Both the GOES imagery and FNOC surface pressure analysis revealed a developing synoptic low pressure system whose position coincided with the maximum in the SASS isotach pattern in the western half of the study region (Fig. 10b). The FNOC isotach analysis showed a wind speed maximum near about 170W which corresponded with an increase in the pressure gradient between a high pressure ridge extending north along an axis at approximately 160W (south of the study region) and the developing low. Since there is sufficient data coverage by SASS west of 175W and SASS makes direct observations that have been shown to be otherwise reliable, the maximum wind speed region portrayed by the SASS isotach pattern is believed to be more reliable than the FNOC model analysis. However, east of 175W the SASS field has a gap coincident with the area of increased pressure gradient.

The atmospheric systems associated with the isotach maxima on Day 16 are on a smaller scale than those on Day 2. However, these results illustrate the advantage of using SASS for sensing atmospheric events at and below the synoptic scale. This capability of SASS in turn

contributes to weak agreement with the lower resolution FNOC wind field.

c. Discussion of Results

By studying the best and worst cases as well as other periods shown in the Appendix, two factors stand out. First, reduced pattern correlations and high RMS errors primarily result from low percentage of coverage by the SASS wind fields before interpolation. The large data gap in the worst case SASS field was the primary reason it compared poorly with the FNOC field, whereas the best case had little or no data gap. The second factor which appears to contribute to variations in correlation between the fields is the difference between the spatial resolution of the fields. The SASS field has a higher spatial resolution which causes it to show features unresolved by the FNOC fields. When the study region is dominated by a synoptic pattern, the isotach fields compare very well. The comparison is not good when there are strong mesoscale smaller scale disturbances within the study region. The ability of SASS to directly measure winds lends credibility to the accuracy of the higher resolution SASS winds when and where they are sensed.

In addition, examination of the figures available in the Appendix shows that the orientation of the SASS data gaps in relation to the wind speed gradient appears to be a significant consideration. Interpolating

across an elongated gap will be more effective when the length of any single contour passing through the gap is minimized. This ensures that both curvature changes in the contour and gradient change across the adjacent contours are more likely to be resolved. Alternately, interpolation across an elongated gap which is oriented parallel to the local gradient in the field is more reliable than interpolation with the gap oriented perpendicular to the local gradient. This is important because the data gaps present in the daily SASS fields are primarily caused by changes in operational mode; therefore, these gaps are consistently oriented north-south. Mean wind speed gradients on the synoptic scale are generally oriented north-south, while mesoscale disturbances may include strong east-west gradients. So, when mesoscale disturbances are sensed, their orentation to data gaps may cause considerable error in the interpolated values. Thus the orientation of data gaps and the percentage coverage of the SASS fields both degrade SASS's capability to resolve mesoscale events. Both of these factors should influence selection of an optimal number of satellites and their orbit trajectories in future observing systems.

5. Wind Stress Comparison

The wind stress on the ocean is the average turbulent transfer of horizontal momentum across the air-ocean interface by the vertical component of the turbulence,

$$\tau = \rho \, \overline{(u' \, w')} = \rho \, u_*^2 \qquad (1)$$

where u' and w' are the variations from the mean horizontal and vertical surface velocities, and ρ is the density of water. The surface friction velocity, u_*, is the scale of the turbulent velocity in the upper part of the ocean mixed layer. The surface stress can be related to the mean wind speed using the bulk formula,

$$\tau = (\rho_a / \rho) \, C_D \, \bar{u}^2 \qquad (2)$$

where C_D is the drag coefficient at the height of the mean wind speed, u and ρ_a is the density of air. The drag coefficient at the sea surface depends on the local sea state, wind speed, and atmospheric stability. This study assumes that the drag coefficient is a function of height above the sea surface only. With this assumption, the variation of wind speed with height directly above the sea surface is a log profile, consistent with the "constant flux" approximation for the atmospheric mixed layer. The wind speed measurements for both data sets are for a height of 19.5m above the sea surface, where a constant drag coefficient of 0.0013 is assumed for use in the ocean model.

Garwood's (1977) ocean mixed layer model uses wind speeds at any height above the surface, but the drag coefficient needs to be adjusted approximately. Therefore, based on a log profile for the change in wind speed with height above the surface the equivalent drag coefficient at 10 m is 0.0015.

Fig. 11 is a scatterplot on a log-log scale of the surface stresses calculated from the SASS and FNOC wind fields. It is important to compare these fields directly because of the non-linear relationship between the wind speed and the surface stress. Fig. 11 shows a good correlation between the surface stress fields. The scatter is relatively small for large values of the stress. The points are close to and relatively symmetrically distributed about the line of perfect correlation. This indicates good overall agreement between the SASS and FNOC wind stress values, especially for average to high wind stress values. The scatter becomes larger for wind stress values below 0.01 dynes/cm^2. However, this constitutes less than 1% of all the data points. Thus, these wind stress values derived from the SASS and FNOC fields are quite similar.

B. CONCLUSIONS

This study has compared the SASS and FNOC wind fields and their utility for ocean mixed layer modeling. These fields have very different possible error sources, stemming from their respective methods of data acquisition and analysis. Even after imposing quality control restrictions, the SASS wind fields suffered from several factors: the use of an empirical algorithm to derive wind speed, the inaccuracy of interpolating to fill data gaps, and differences between the magnitudes of aliased wind vector measurements. The FNOC wind field accuracy suffers from a lack of sufficient numbers of observations over large ocean regions, compounded by the limitations of atmospheric model physics introduced by simplifying assumptions. In light of these widely differing possible sources of error, it is significant that these fields agree as well as they do, lending credibility to both methods. In particular, the verification by the FNOC wind fields of the accuracy of the SASS wind measurements when averaged spatially and temporally indicates the potential of the scatterometer wind measurements for ready use in any ocean mixed layer model which does not require wind direction.

The ocean mixed layer model used in this study was very sensitive to the variations of the wind fields used as boundary conditions. The accuracy required by the model is higher than the verifiable accuracy of either wind field.

VI. CONCLUSIONS AND RECOMMENDATIONS

A. SUMMARY OF RESULTS

It has been shown that with quality control restrictions carefully imposed on the SASS data set, the SASS wind measurements compare very well in phase and magnitude with the FNOC wind measurements over a large ocean region on a grid which resolves the synoptic scale. The primary cause of poor comparisons were the occasionally large data gaps in the SASS wind fields which were filled by interpolation. These gaps were largely attributable to changes in the SASS operational mode during data acquisition.. A secondary cause of weak comparison was the inability of the FNOC wind fields to resolve events on spatial scales as small as those resolved by the SASS wind fields. There was shown to be no significant difference or bias between the wind stress values derived from the SASS and FNOC fields. A comparison of ocean model simulations using the two wind fields in Garwood's model (1977) revealed a high sensitivity by the model to any variations in synoptic scale wind fields.

shallowing rates. This may be due to the model's technique for deepening, which is done in several smaller time increments according to the TKE available during the time step for mixing, as compared to that used for shallowing, which is done in one calculation for the time step.

Therefore, the consistent accuracy of synoptic scale winds used for forcing ocean mixed layer models is an extremely important factor in accurately predicting synoptic scale changes in MLD. The results of this study imply the importance of accurate surface heat fluxes. See Jaramillo (1984) for a more complete discussion. Also, the dependence of ocean synoptic scale MLD predictions on both the wind stress boundary condition and the current MLD indicates the importance of the accuracy and resolution of the initial thermal structure fields.

likely to bring the simulated MLD changes into magnitude and phase agreement.

D. DISCUSSION OF RESULTS

Primarily, these results show that the model is very sensitive to the variations in the wind speed boundary condition. Although the wind fields were similar by direct comparison, the differences when used as model forcing are significant. This illustrates the importance of accurate wind speed measurements for ocean mixed layer model use. The results also indicate the importance of not only the wind speed accuracy, but also the consistency of its accuracy throughout the forecast period. The model will maintain a "record" of these wind speed inaccuracies during each subsequent time step of the simulation after they have been introduced because of their effect on the thermal structure. Thus, differences appear to be cumulative, causing divergence in the mixed layer calculations.

The results demonstrate that the wind speed boundary condition in this study is the primary forcing mechanism influencing the synoptic scale changes in MLD. This result, however, should be expected since the climatological heat flux boundary conditions used in this study do not contain synoptic scale fluctuations. Additionally, the inaccuracies appeared to be less influential on MLD changes when they altered deepening rates than when they altered

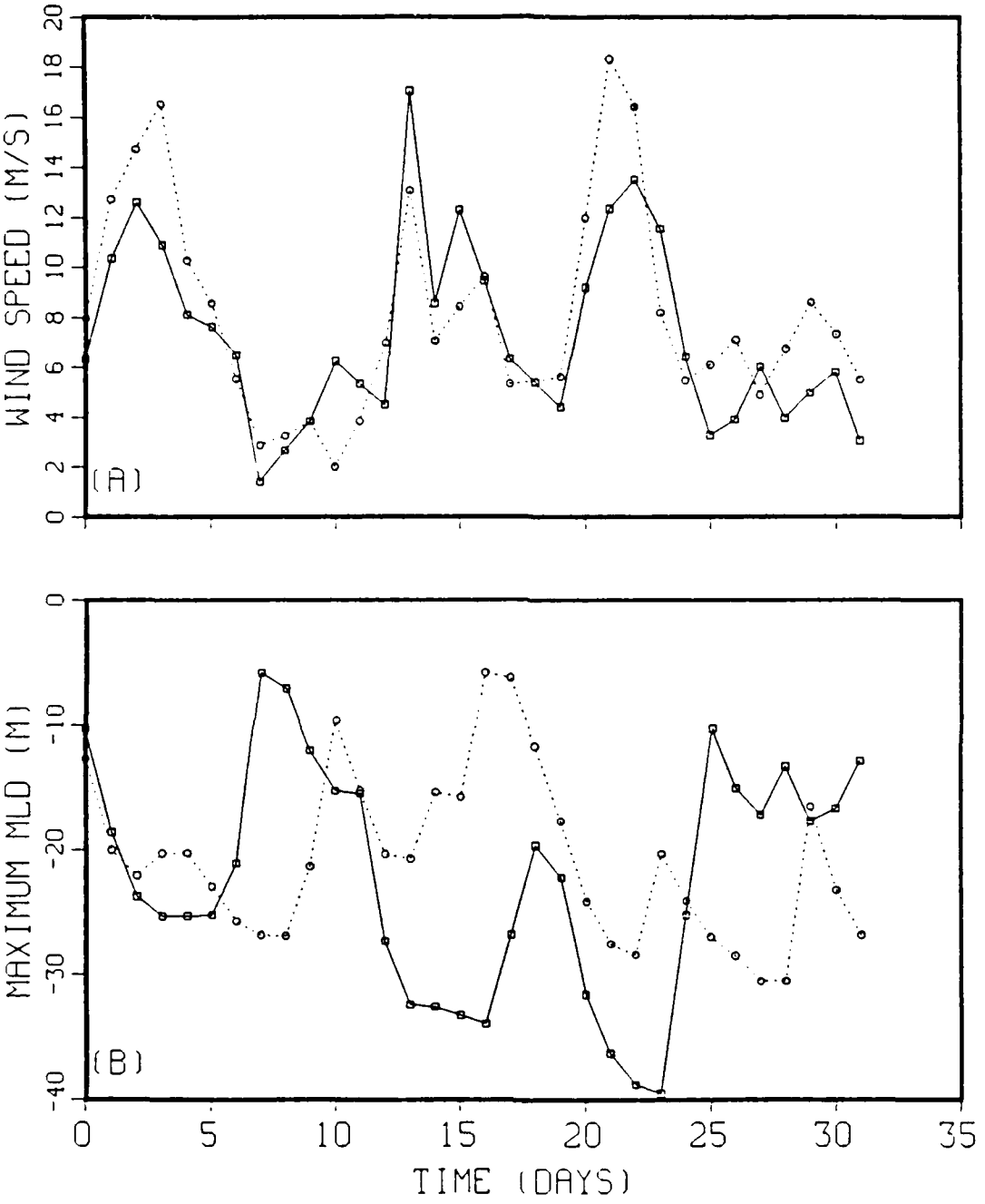

Figure 15. Same as Fig. 13 at location 42N, 155W.

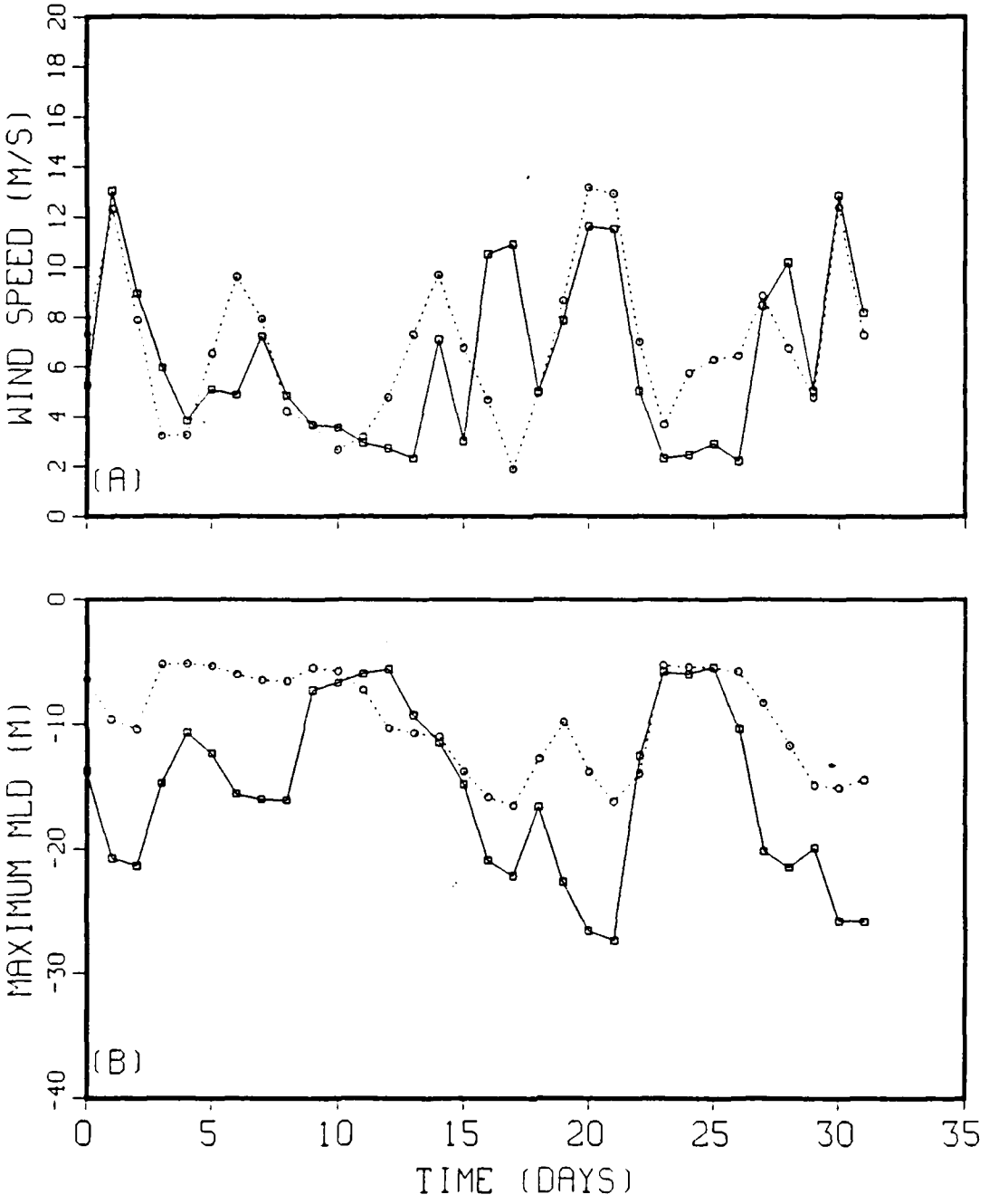

Figure 14. Same as Fig. 13 at location 40N, 175W.

structure so that the subsequently similar wind stress forcing produced very different changes in MLD.

2. Location 40N, 175W

This location was chosen because it was in the region where the SASS and FNOC isotach fields shown in the Appendix differed the most over the 30 day period. The results in Fig. 14 show model sensitivities similar to those found in Fig. 13. The first four days show a very good agreement between the wind fields and the resulting phase agreement between the simulated MLD's. Although the wind speeds diverged sharply for short time periods, sometimes causing large differences between the fields, the MLD simulations remained remarkably well in phase throughout the time series. This result indicates that the duration of the difference in the wind speeds is an important consideration in the model's sensitivity to these changes.

3. Location 42N, 155W

This location was chosen to coincide with the region of maximum cooling on both forecast fields. The results at this location are shown in Fig. 15. These results also indicate the importance of a consistently accurate wind speed measurement for ocean mixed layer modeling. Once the wind speed measurements differ, the thermal structure in and below the mixed layer is altered and no subsequent correlation between the wind speeds is

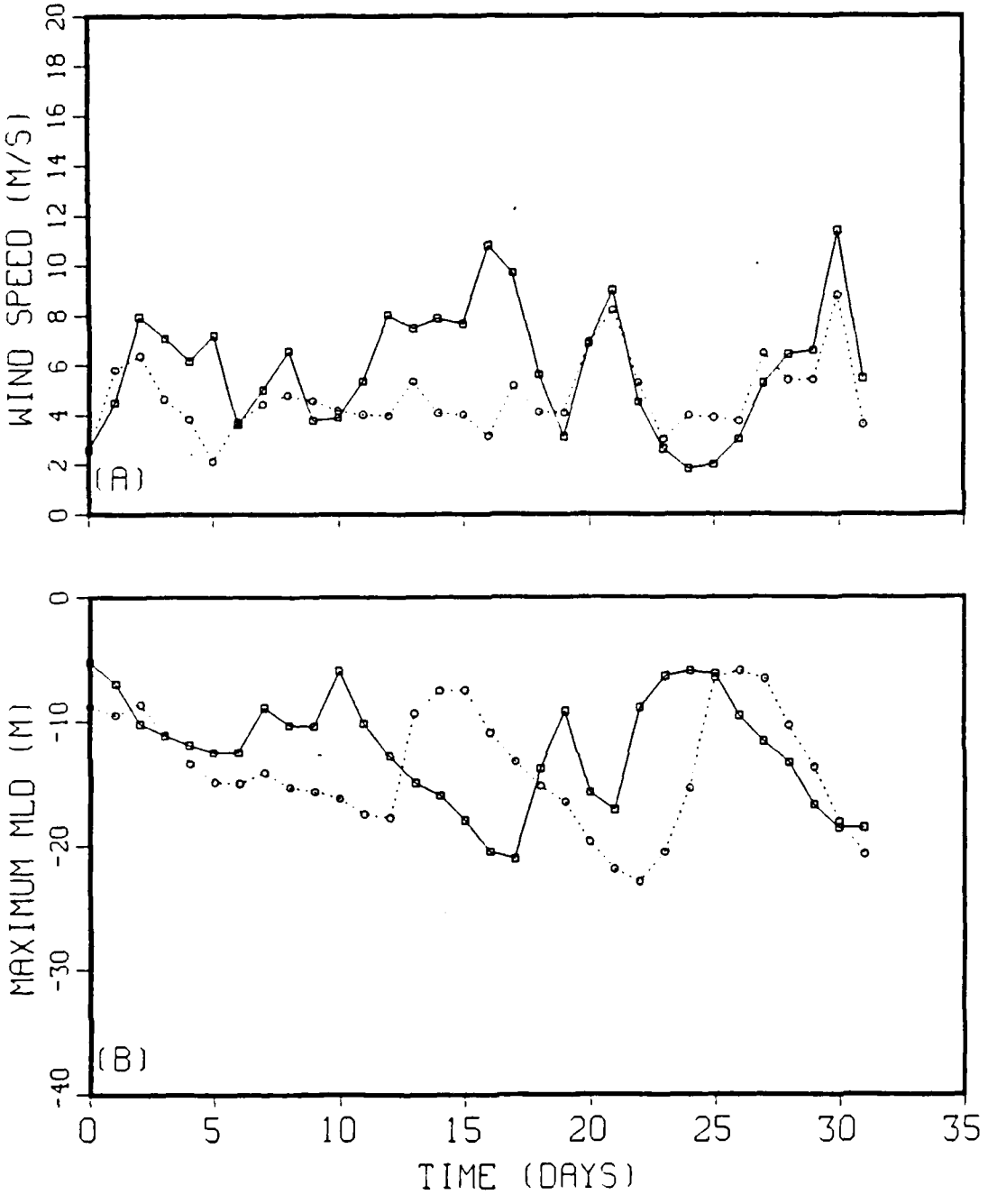

Figure 13. (a) Time series of SASS (solid) and FNOC (dotted) wind speeds during 30 day simulation at 36N, 180. (b) Same as (a) for maximum mixed layer depth per 24 hour period.

conditions that was unexpected in light of the seemingly small differences in wind speed shown in Fig. 7.

C. TIME SERIES OF 30 DAY SIMULATION

To further investigate the reasons for the differences in the 30 day temperature change fields between SASS and FNOC forcing, three locations were chosen for time series comparisons.

1. Location 36N, 180W

This location was chosen to coincide with a warming region in both simulated fields. Fig. 13 is a plot of the time series of wind speed and daily maximum mixed layer depth, for both SASS and FNOC forcing.

From the results presented in Fig. 13, the model's sensitivity to wind speed differences as large as 4 m/s is shown. Fig. 13 illustrates that once the MLD predictions differ significantly due to differences in the wind speed, any subsequent agreement between the MLD forecasts is likely to be only coincidental. This results because the forecast of the MLD change is dependent on the current MLD. As the MLD grows, it erodes the thermal structure below the mixed layer, which, in turn, reduces the rate of further deepening. This is best illustrated during the five days following Day 17. During this time, the wind speeds correlate very well, but the changes in MLD do not. The days preceeding Day 17 sufficiently altered the thermal

when FNOC fields were used. This prediction of net cooling is unlikely for the July to August time frame in the North Pacific. However, it is unlikely that the wind stress boundary condition was to blame, because both wind fields created similar trends. It is more probable that the cooling was caused by some other forcing variable. Possibly suspect are the heat flux fields since they are a 20 year climatological average whereas the wind fields and the initial ocean thermal structure are not. Also suspect is the initialization field which may not have sufficient vertical resolution to adequately depict the initial gradient of the thermocline region. This underestimate of the initial tangential gradient would decrease the amount of TKE needed to deepen the mixed layer, which would cause the MLD to increase too much, lowering the mixed layer temperature. A preliminary investigation indicates that the initial temperature structure fields may be the primary cause of the unseasonable cooling simulated.

Regardless of the reason for the cooling trend, the wind fields may still be compared by way of model output because all other model variables remained unchanged during the simulations. Fig. 12 shows that the wind fields produce similar patterns. The maximum cooling and warming takes place in the same regions. However, these results show a sensitivity to changes in the wind stress boundary

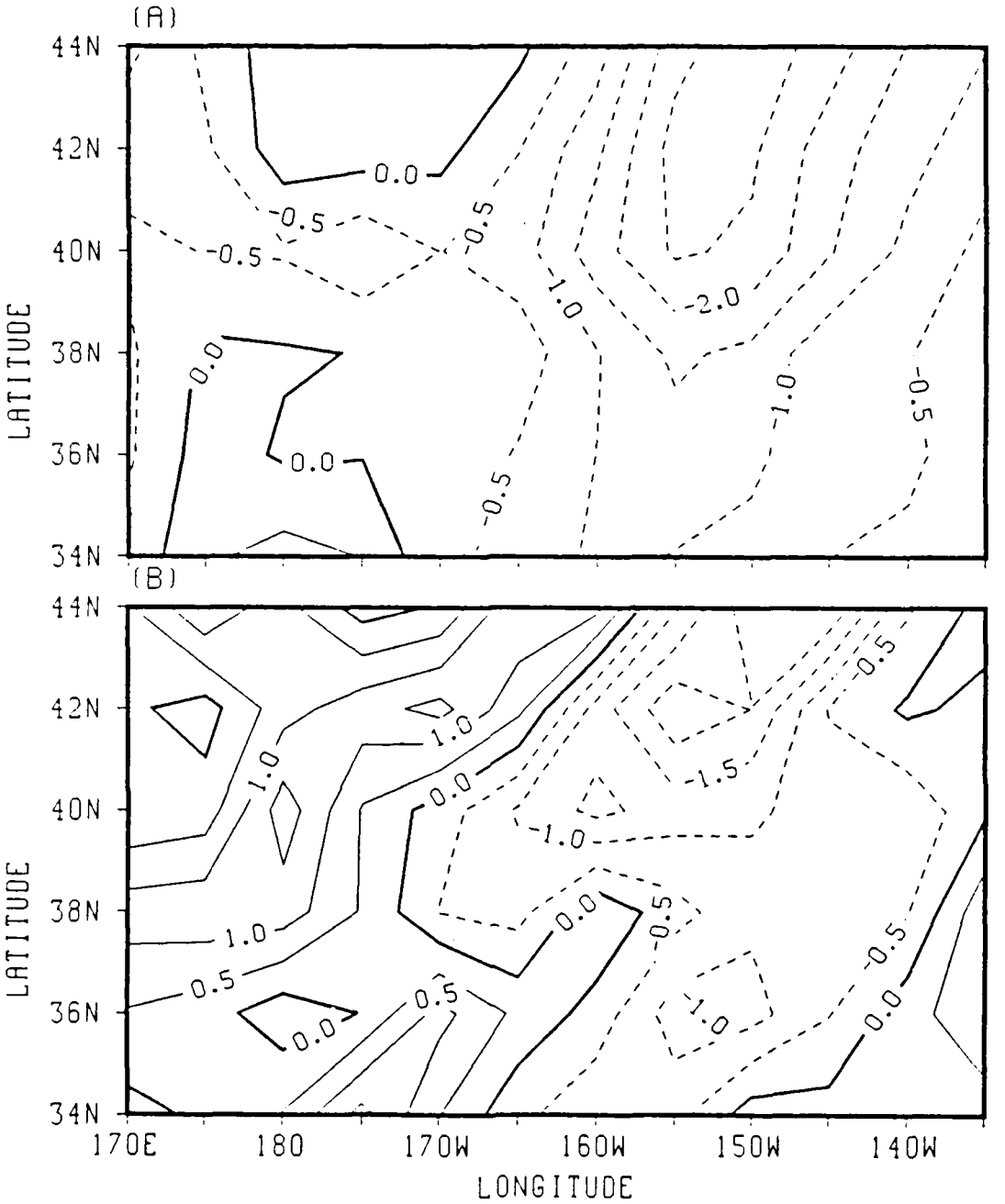

Figure 12. (a) 30 day model simulation of temperature change (°C) July 15 to August 15 at sea level using SASS wind stress boundary condition. CI = 0.5. (b) Same as (a) for FNOC wind fields.

erodes the underlying stable water mass, deepening the mixed layer. The mixed layer shallows when there is insufficient TKE to deepen or maintain the current mixed layer depth against the existing thermocline and a positive buoyancy flux into the layer.

Since the model depends on the interaction between the heat and momentum fluxes to determine the amount of TKE available for changing the mixed layer depth (MLD), it is important that the phase and magnitude of the surface wind forcing and surface heating be properly represented in the data sets used for model boundary conditions. Also, it is important that the data set used to initialize the model's thermal structure portray accurately the thermocline region below the mixed layer. The steepness of the temperature gradient in the thermocline region will determine the amount of available TKE necessary to deepen the mixed layer a given amount.

B. 30 DAY SIMULATION

A 30 day simulation of the mixed layer was performed both with the SASS wind fields and with the FNOC wind fields. The initial sea surface temperature fields were subtracted from the resulting 30-day simulation fields to yield the temperature change fields shown in Fig. 12.

The model predicted cooling over most of the region when the SASS winds were used and over about half the region

V. MODEL COMPARISON

A. MODEL PHYSICS

The model used in this study, described in detail by Garwood (1977), is a second order closure, bulk turbulent kinetic energy (TKE) model which separately retains the horizontal and vertical TKE equations. The model forcing consists of the surface fluxes of momentum and buoyancy. The surface momentum flux increases the horizontal TKE through the interaction of the surface stress with the vertical shear of the mean current. The buoyancy flux is produced by latent and sensible heat exchange, long wave radiation at the surface, heating by solar radiation throughout the euphotic zone and the exchange of heat at the mixed layer's lower boundary by entrainment. The model assumes that the vertical turbulent velocity (scaled from the vertical TKE) within the mixed layer transports the surface generated TKE to the entrainment zone. The rate of entrainment of cooler water within and below the thermocline is proportional to the amount of vertical TKE within the layer. The vertical TKE is created by the redistribution of horizontal TKE from pressure rate of strain action, or by surface cooling, and it is decreased by dissipation and entrainment. The TKE available in the entrainment zone

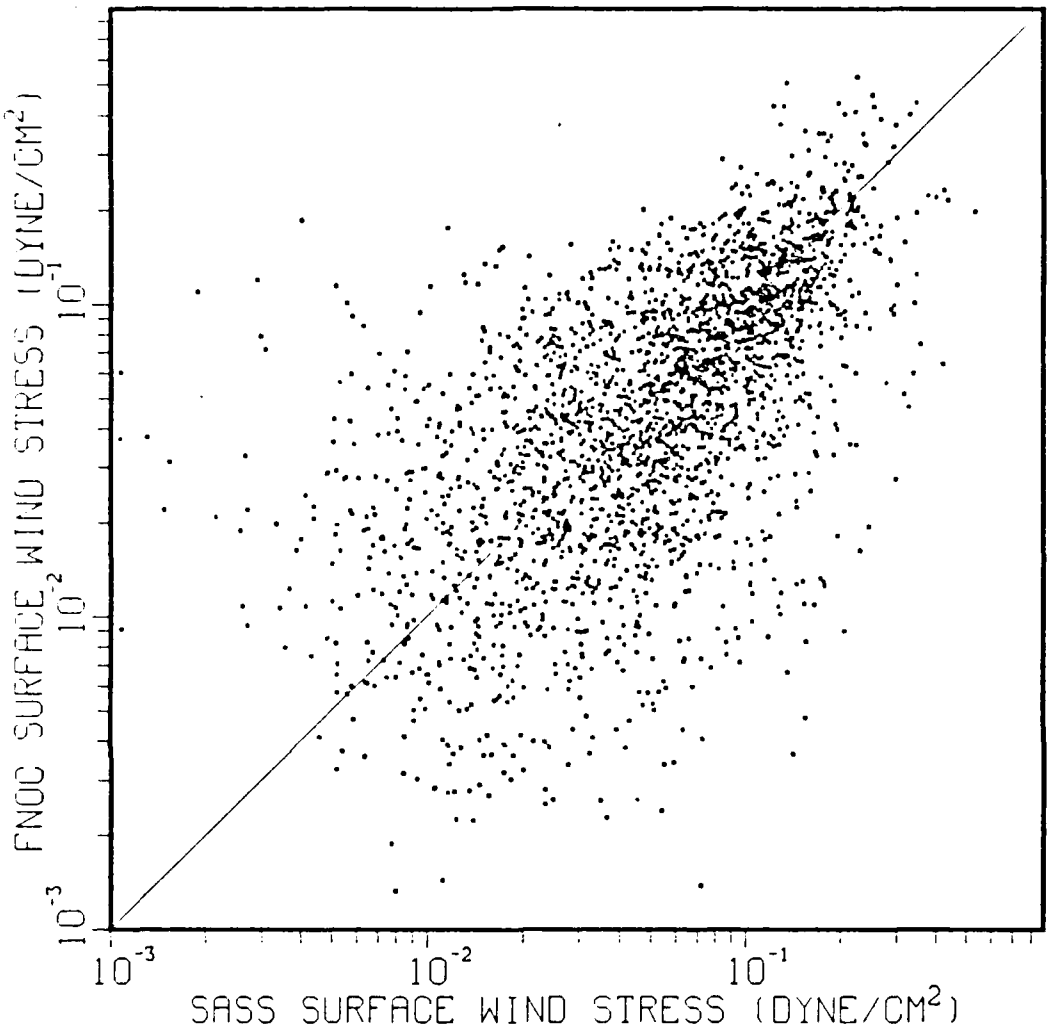

Figure 11. Scatterplot on log-log scale of surface stress values computed from SASS and FNOC surface wind speed fields. The diagonal is included for bias detection.

However, though the sensitivity of the model to the wind field has been shown, it should be noted that monthly forecast accuracy is limited even more by difficulties in specifying the heat flux boundary condition and in the initialization fields. The SASS fields do provide wind fields which are comparable to the FNOC wind fields and which may be used as an alternative data source for further study of the ocean mixed layer model's response to wind forcing.

Perhaps the most promising aspect of this study's results is that it creates a basis for combined use of SASS and FNOC wind fields. While studying the impact of scatterometer data on weather prediction model forecasts, Atlas et al. (1982) referred to this potential in their conclusions:

> "Regional studies demonstrate that synoptic and subsynoptic systems which are not detected or poorly analyzed are accurately represented in scatterometer data, and short-range forecasts based on this data should be improved."

While SASS has the potential to significantly improve the detection and analysis of subsynoptic and synoptic systems, the use of a dynamic model to fill gaps in the SASS coverage would be a substantial improvement over non-selective use of polynomial interpolation. The potential for combining the SASS data and standard atmospheric analyses is promising for ocean mixed layer model applications because of the symmetry of the wind stress

scatterplot comparison. indicating that both wind fields produce comparable wind stress values.

Additionally, the scatterometer scheduled to be on board the NROSS satellite should increase the potential of this data source (Satellite Surface Stress Working Group, 1982). It will be capable of reducing the directional ambiguity in measured wind vectors, as well as providing a spatial resolution of 25km. Also, should it complete its three year operational mission, it will provide improved data coverage by operating in a double side swath mode continuously and by increasing and stabilizing the average width of side swaths. Operation in the double side swath mode could easily reduce the time period required to produce adequate coverage for interpolation to 12 hours or less. Furthermore, FNOC now uses a more advanced operational atmospheric model, the Naval Operational Global Atmospheric Prediction System (NOGAPS), which may improve both the coverage and quality of both the surface winds and the surface heat fluxes over the oceans.

C. RECOMMENDATIONS

It is recommended that further study using the SASS data set, available from JPL, with Garwood's ocean mixed layer model (1977) concentrate efforts on three areas. The first is an extension to this study, which explores in more detail the model's sensitivity to the synoptic variations of

the wind speed boundary condition. The SASS fields have the potential for synoptic mixed layer modeling use in related areas of the reduced ADS region. A more formal statistical analysis of the SASS wind fields using time-space objective analysis methods may enhance this potential. The second effort is to develop an acceptable method for combining the SASS and FNOC fields and using the combined field for model forcing. Finally, using SASS and FNOC wind fields, a study of the relationship between the model's response to synoptic and mesoscale forcing is in order. An investigation of the potential of using local synoptic forecasts combined with regional mesoscale forecasts may aid in this study.

Should the NROSS scatterometer make longer time period data sets available, a similar comparison study using a large number of monthly forecasts should be made to determine quantitatively the differences in the model's response to the scatterometer and FNOC (NOGAPS) wind fields, including seasonal and regional changes. The NROSS wind fields should allow comparison with a 12 hour time scale. Such studies will require not only NROSS and NOGAPS fields for model forcing, but also ocean thermal structure data for model initialization and verification. This and other studies (e.g. Jaramillo, 1984; Stringer, 1984) have shown that the ADS NORPAX analysis is barely adequate. Thus future large scale ocean thermal structure analyses will

have to be improved if ocean model forecasts are to be improved.

APPENDIX A

SASS AND FNOC COMPARISON

The following pages present figures which compare SASS data coverage before interpolation and SASS and FNOC isotach analyses for the 34 day period of this study. The figures are similar to Fig. 11 and are arranged four to a page. Table A-1 lists the date corresponding with day shown for each figure.

TABLE A-1
List of Time Periods Studied

DAY	JULIAN DAY	DATE
1	197	Jul 16
2	198	Jul 17
3	199	Jul 18
4	200	Jul 19
5	201	Jul 20
6	202	Jul 21
7	203	Jul 22
8	204	Jul 23
9	205	Jul 24
10	206	Jul 25
11	207	Jul 26
12	208	Jul 27
13	209	Jul 28
14	210	Jul 29
15	211	Jul 30
16	212	Jul 31
17	213	Aug 1
18	214	Aug 2
19	215	Aug 3
20	216	Aug 4
21	217	Aug 5
22	218	Aug 6
23	219	Aug 7
24	220	Aug 8
25	221	Aug 9
26	222	Aug 10
27	223	Aug 11
28	224	Aug 12
29	225	Aug 13
30	226	Aug 14
31	227	Aug 15
32	228	Aug 16
33	229	Aug 17
34	230	Aug 18
35	231	Aug 19
36	232	Aug 20
37	233	Aug 21
38	234	Aug 22
39	235	Aug 23
40	236	Aug 24
41	237	Aug 25
42	238	Aug 26

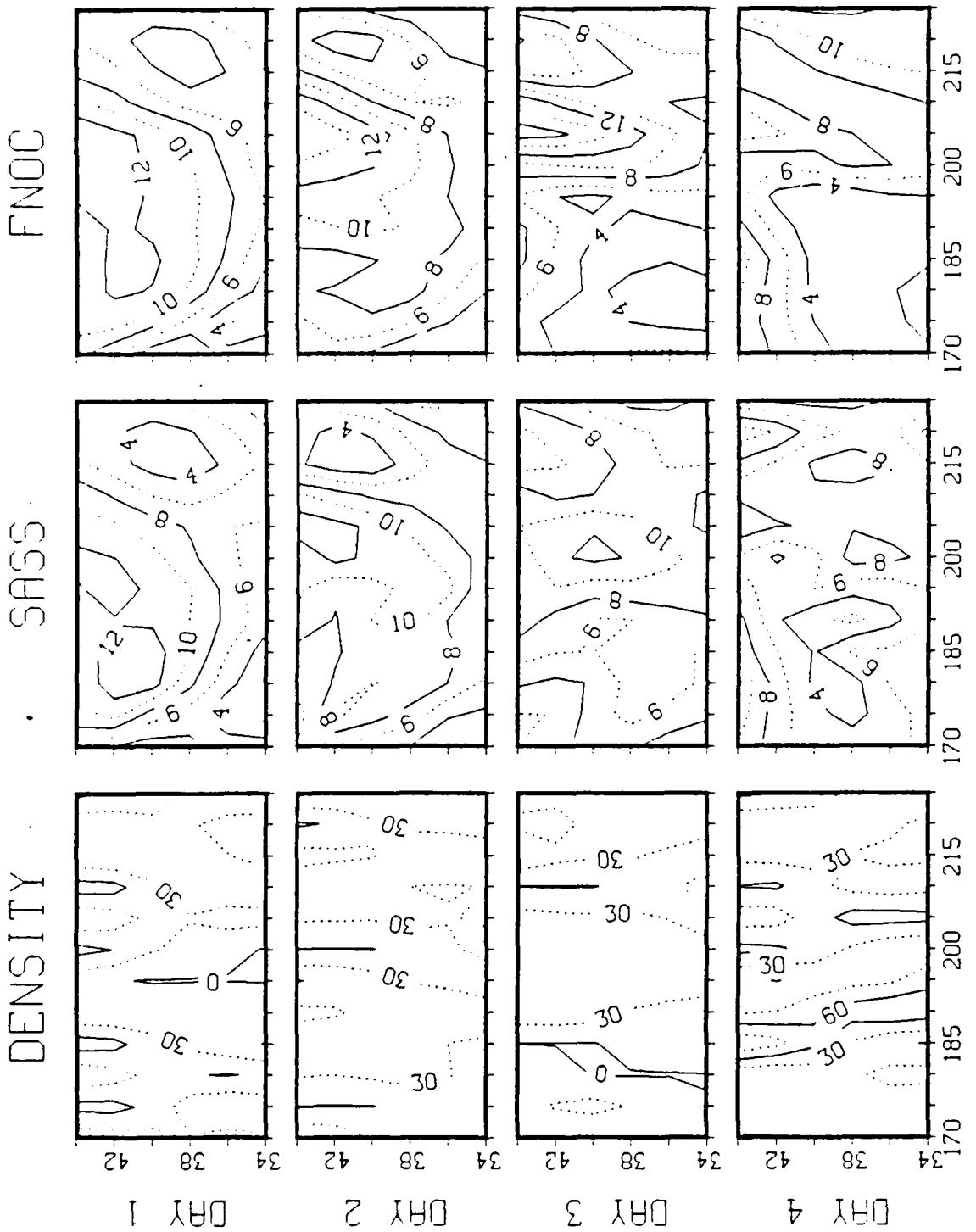

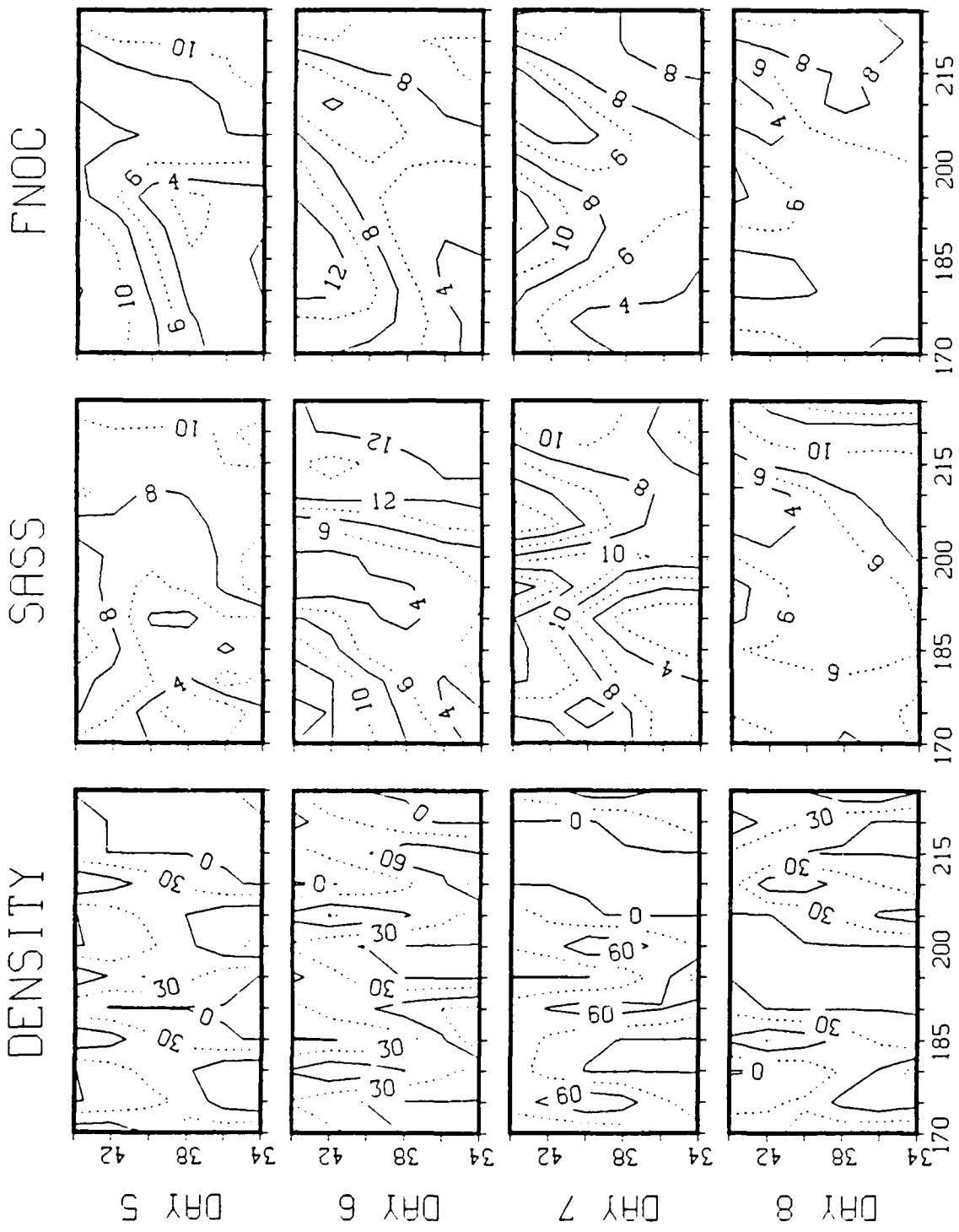

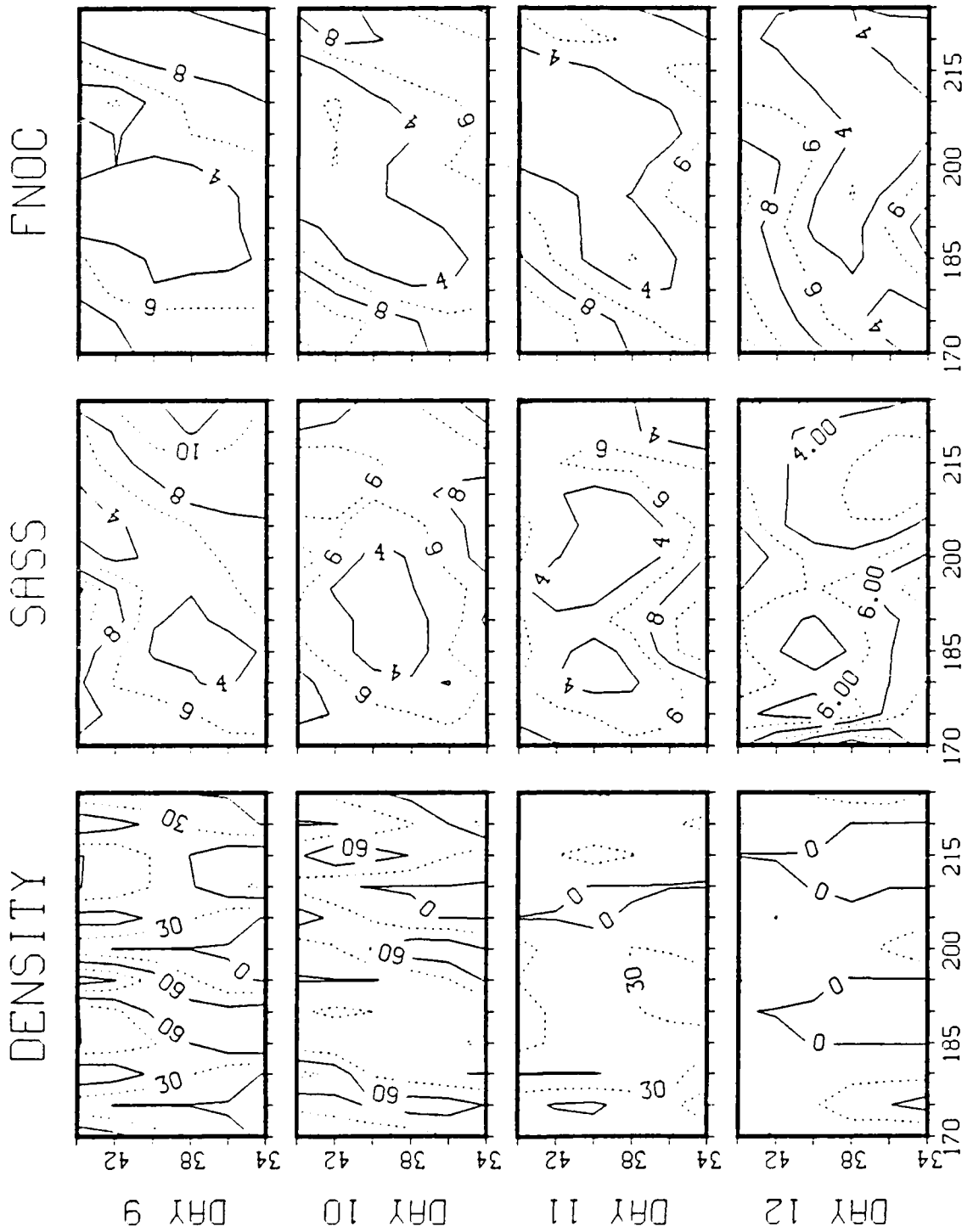

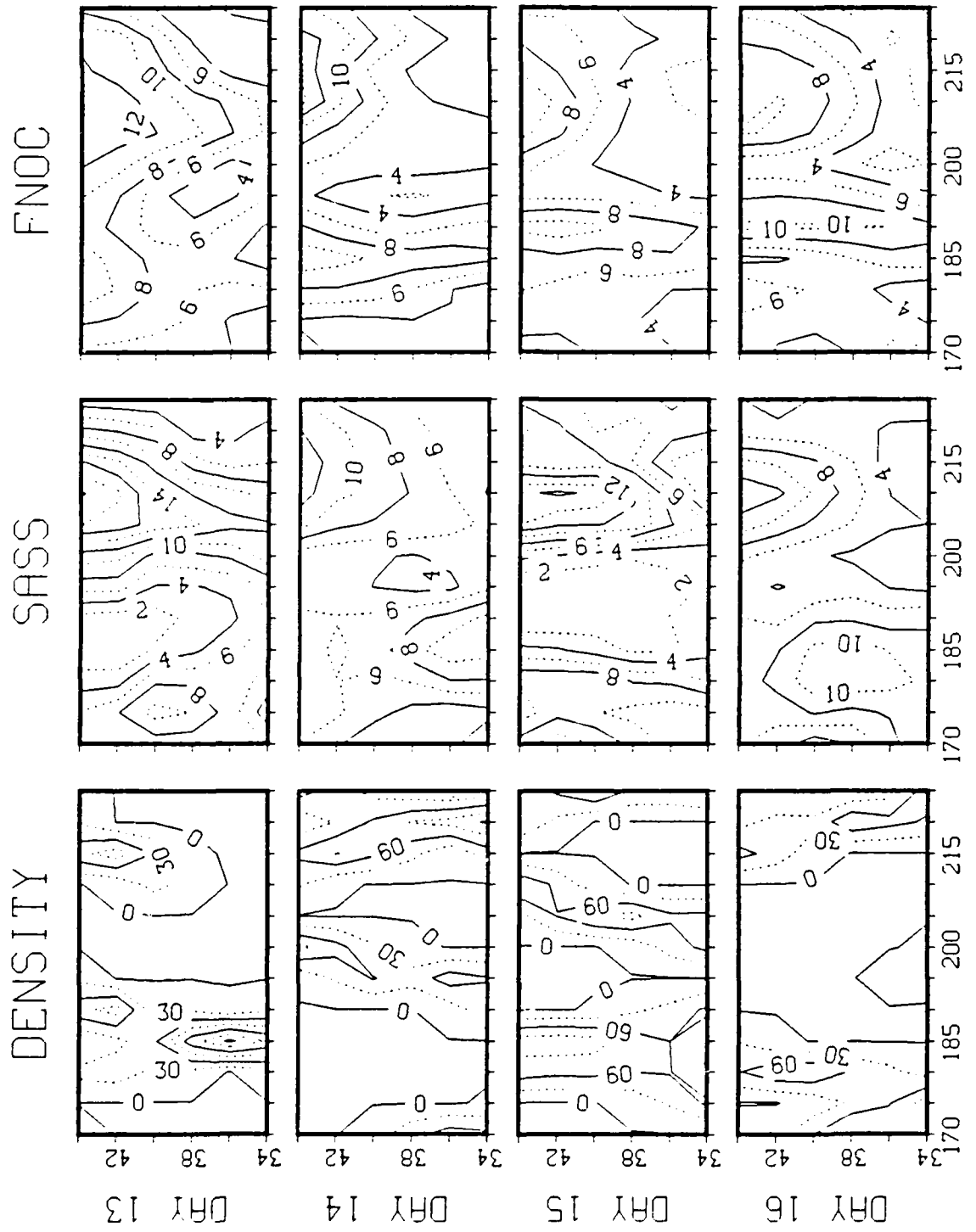

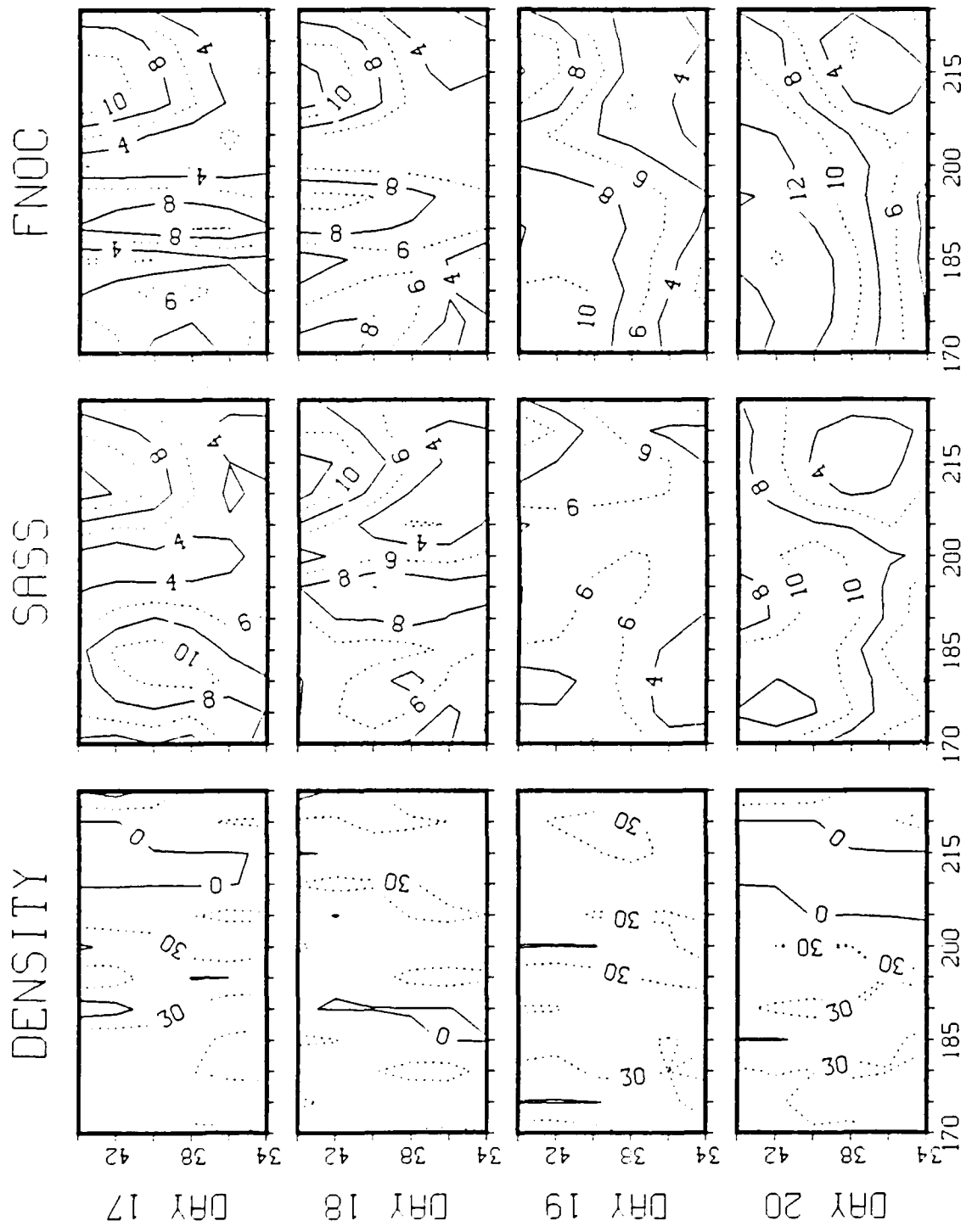

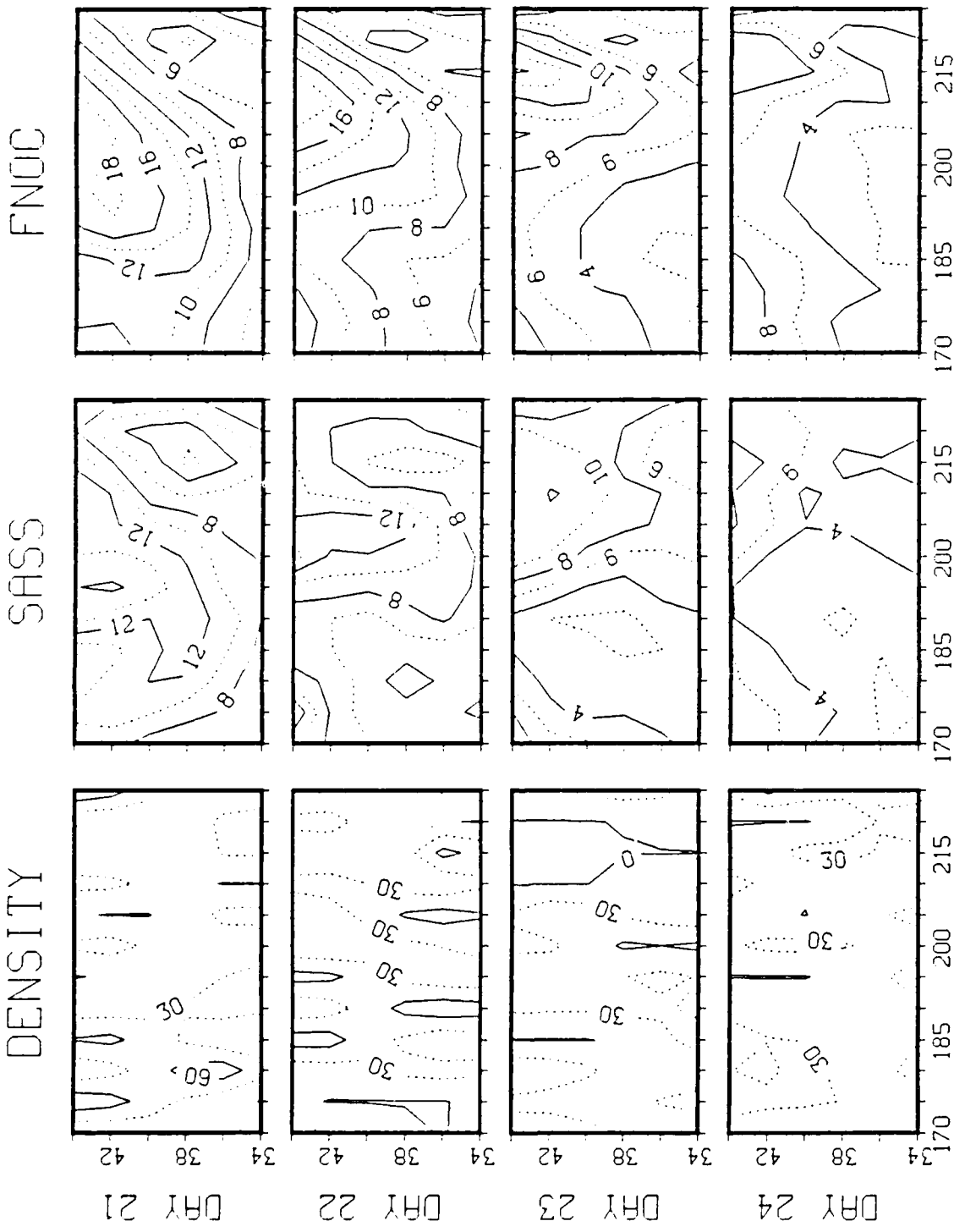

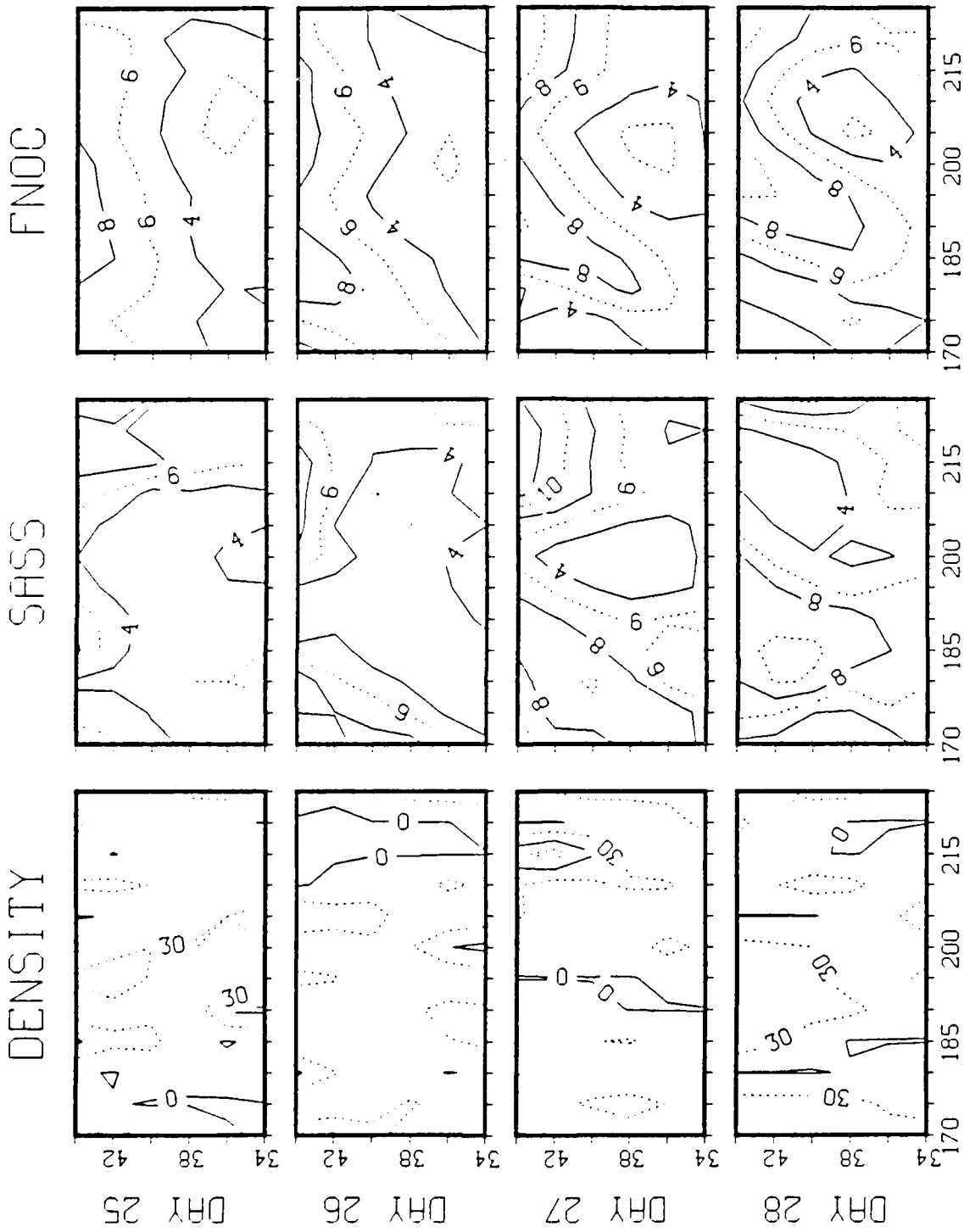

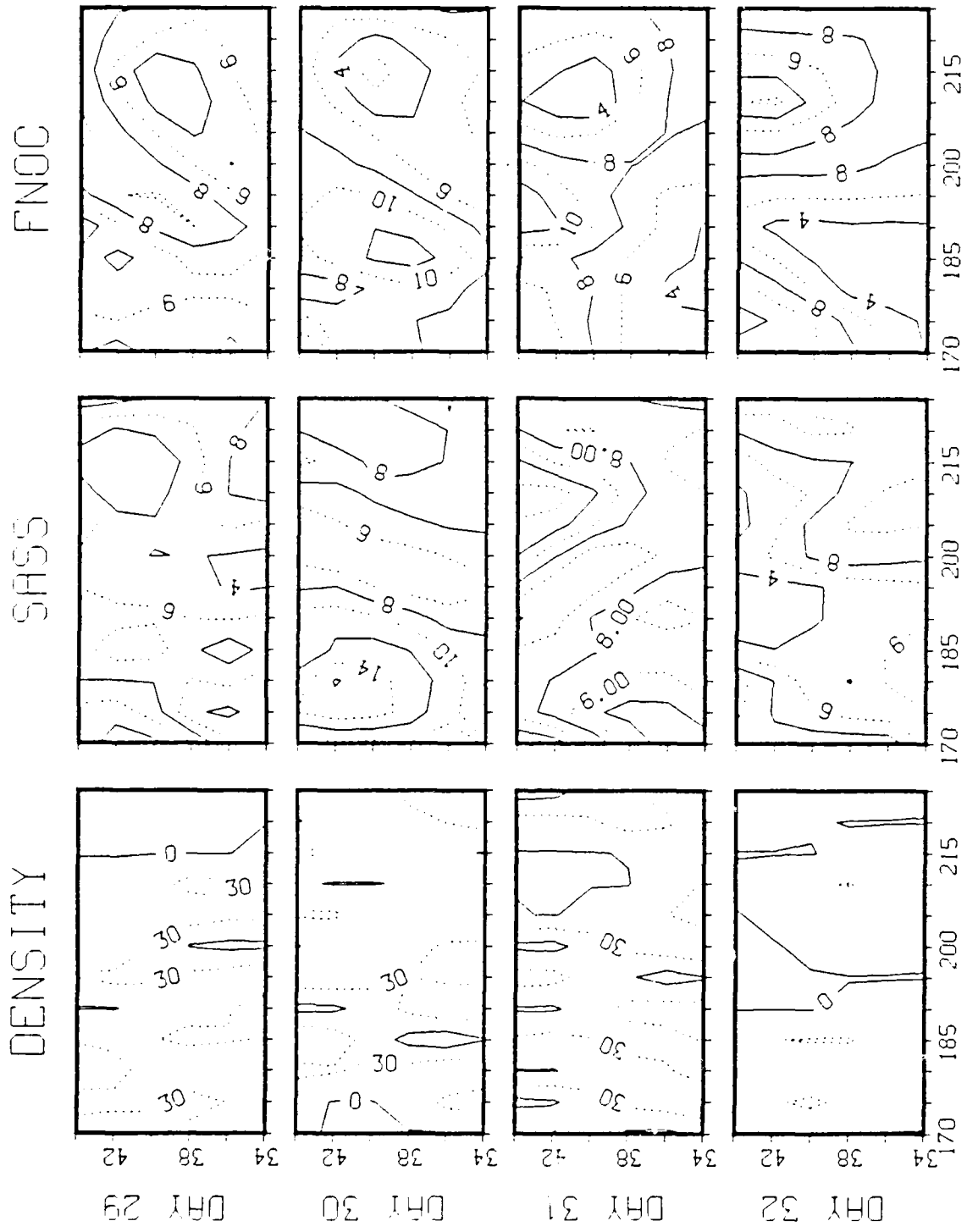

AD-A153 748 UTILIZATION OF THE SEASAT SCATTEROMETER WINDS FOR OCEAN MIXED LAYER MODELING(U) NAVAL POSTGRADUATE SCHOOL MONTEREY CA E J COOLBAUGH DEC 84 2/2

UNCLASSIFIED F/G 8/3 NL

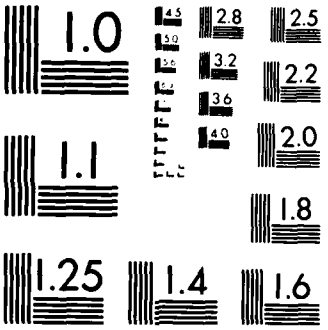

MICROCOPY RESOLUTION TEST CHART
NATIONAL BUREAU OF STANDARDS 1963-A

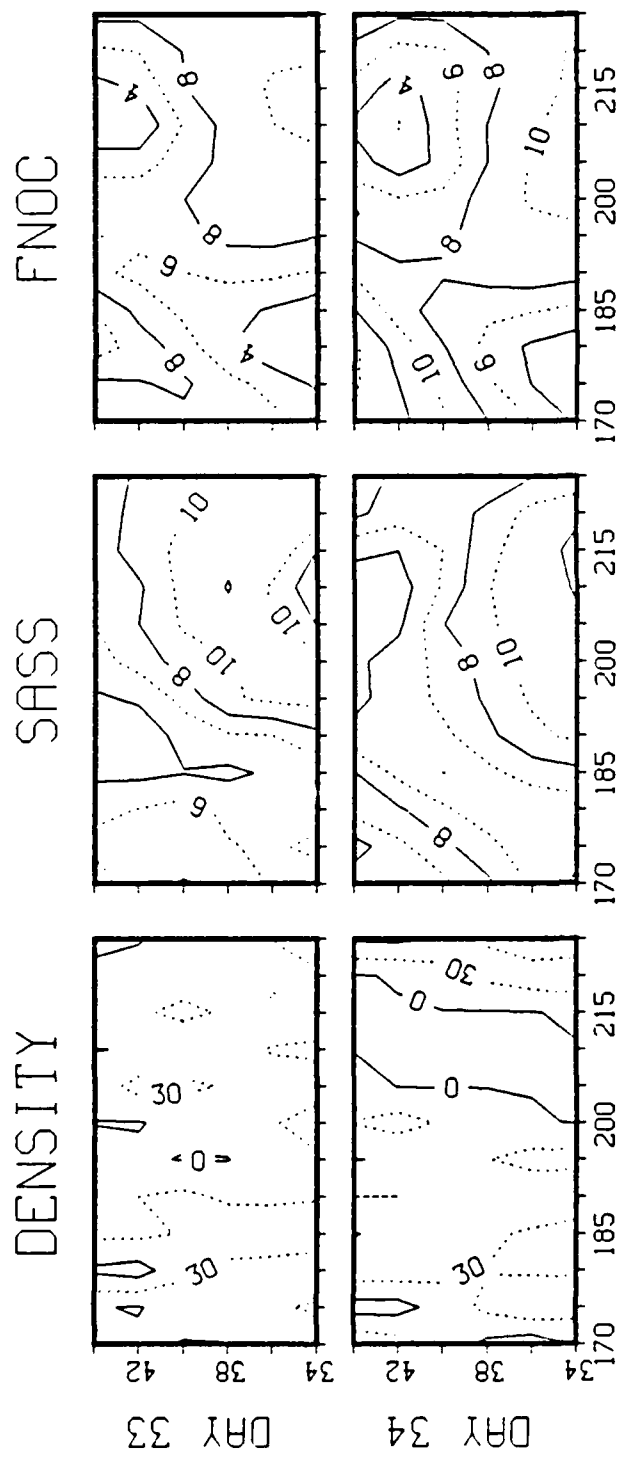

LIST OF REFERENCES

Atlas, R., S. Peteherych, P. Woiceshyn, M. Wurtele, 1982: Analysis of satellite scatterometer data and its impact on weather forecasting. IEEE, 0197-7385, 415-420.

Boggs, D.H., 1982: SEASAT Scatterometer Geophysical Data Record Users Handbook. NASA, JPL D-129, 210 pp.

Brown, R. A., V. J. Cardone, T. Guymer, J. Hawkins, J. E. Overland, W. J. Pierson, S. Peteherych, J. C. Wilkerson, P. M. Woiceshyn, and M. Wurtele, 1982: Surface wind analysis for SEASAT. J. Geophys. Res.,87,No.C5, 3355-3364.

Brown, R.A., 1983: On a satellite scatterometer as an anemometer. J. Geophys. Res., 88, No. C3, 1663-1673.

Gallacher, P., R. Garwood, R. L. Elsberry and A. Bird, 1983: A determination of the constants for a second-order closure turbulence model from geophysical data. Rep. No. NPS63-83-004, Naval Postgraduate School, Monterey.

Halberstam, I., 1980: Some considerations on the evaluation of SEASAT-A scatterometer (SASS) measurements. J. Phys. Oceanogr., 10, 623-632.

Hawkins, J.D. and P.G. Black, 1983: SEASAT scatterometer detection of gale force winds near tropical cyclones. J. Geophys. Res., 88, No.C3, 1674-1682.

Jaramillo, Ben J., 1984: One-dimensional model hindcasts of warm anomalies in the North Pacific Ocean. M.S. Thesis, Naval Postgraduate School, 82 pp.

Jones, W. L., L. C. Schroeder, D. H. Boggs, G. J. Dome, E. M. Bracalente, R. A. Brown, W. J. Pierson, and F. J. Wentz, 1982: The SEASAT-A satellite scatterometer: The geophysical evaluation of remotely sensed wind vectors over the ocean. J. Geophys. Res., 87, No.C5, 3297-3317.

Moore, R. K., I. J. Birrer, E. M. Bracalente, G. J. Dome, and F. J. Wentz 1982: Evaluation of atmospheric attenuation from SMMR brightness temperature for the SEASAT satellite scatterometer. J. Geophys. Res., 87, C5, 3337-3354.

Pond, S. and G.L. Pickard, 1978: Introductory Dynamic Oceanography. Pergamon Press Inc., Maxwell House, Farview Park, Elmsford, N.Y., 252 pp.

Satellite Surface Stress Working Group: J. J. O'Brien, R. Kirk, L. McGoldrick, J. Witte, R. Atlas, O. Brown, E. Bracalente, R. Haney, D. E. Harrison, Cdr. D. Honhart, H. Hurlburt, R. Johnson, L. Jones, K. Katsaros, R. Lambertson, S. Peteherych, W. Pierson, J. Price, D. Ross, R. Stewart, P. Woiceshyn, 1982: Scientific opportunities using satellite wind stress measurements over the ocean. Nova University N.Y.I.T. Press, Fort Lauderdale, Florida. 153 pp.

Stringer, Gary L., 1983: One-dimensional model hindcasts of cold anomalies in the North Pacific Ocean. M.S. Thesis, Naval Postgraduate School, 136 pp.

Wentz, F. J., 1977: A two-scale scattering model with application to the JONSWAP '75 Aircraft Microwave Scatterometer Experiment. NASA Contractor Report-2919 under Contract NAS1-14330 for Langley Research Center, Hampton, VA.

White, W. B., R. L. Bernstein, 1979: Design of an oceanographic network in the midlatitude North Pacific. J. Phys. Oceanogr., 9, 592-606.

Wyrtki, K., 1965: The average annual heat balance of the north pacific ocean and its relation to ocean circulation. J. Geophys. Res., 70, No. 18, 4547-4559.

INITIAL DISTRIBUTION LIST

		No. Copies
1.	Defense Technical Information Center Cameron Station Alexandria, Virginia 22314	2
2.	Library, Code 0142 Naval Postgraduate School Monterey, California 93943	2
3.	Commanding Officer Naval Ocean Research and Development Activity NSTL Station, Missisippi 39529	1
4.	Commander Naval Oceanography Command NSTL Station, Mississippi 39529	1
5.	Commanding Officer Fleet Numerical Oceanography Center Monterey, California 93940	1
6.	Officer-in-Charge Naval Environmental Prediction Research Facility Monterey, California 93940	1
7.	Librarian Naval Environmental Prediction Research Facility Monterey, California 93940	1
8.	Office of Naval Research Code 481 NSTL Station, Mississippi 39529	1
9.	Dean of Research, Code 012 Naval Postgraduate School Monterey, California 93943	1
10.	Professor Russell L. Elsberry, Code 63Es Naval Postgraduate School Monterey, California 93943	1
11.	Professor Roland W. Garwood, Jr., Code 68Gd Naval Postgraduate School Monterey, California 93943	2

12. Department of Meteorology, Code 63Mm — 1
Naval Postgraduate School
Monterey, California 93943

13. Professor Robert L. Haney, Code 63Hy — 1
Naval Postgraduate School
Monterey, California 93943

14. Professor Christopher N.K. Mooers, Code 68Mr — 1
Naval Postgraduate School
Monterey, California 93943

15. Professor Robert J. Renard, Code 63Rd — 1
Naval Postgraduate School
Monterey, California 93943

16. Mr. Patrick C. Gallacher, Code 63Ga — 1
Naval Postgraduate School
Monterey, California 93943

17. Professor James L. Mueller, Code 68My — 1
Naval Postgraduate School
Monterey, California 93943

18. Department of Oceanography, Code 68 — 1
Naval Postgraduate School
Monterey, California 93943

19. Commanding Officer — 1
Naval Research Laboratory
Attn: Library, Code 2627
Washington, D.C. 20375

20. Office of Naval Research — 1
Attn: Code 460
800 N. Quincy Street
Arlington, Virginia 22217

END

FILMED

6-85

DTIC